

# Funnel Libraries for Real-Time Robust Feedback Motion Planning

Anirudha Majumdar and Russ Tedrake  
 Computer Science and Artificial Intelligence Lab  
 Massachusetts Institute of Technology  
 Cambridge, MA, USA  
 Email: {anirudha, russt}@mit.edu

August 27, 2021

## Abstract

In this paper we consider the problem of generating motion plans for a robot that are guaranteed to succeed despite uncertainty in the environment, parametric model uncertainty, and disturbances. Furthermore, we consider the case where these plans must be generated in real-time, because constraints such as obstacles in the environment may not be known until they are perceived (with a noisy sensor) at runtime. Previous work on feedback motion planning for nonlinear systems was limited to offline planning due to the computational cost of safety verification. Here we augment the traditional *trajectory library* approach by designing locally stabilizing controllers for each nominal trajectory in the library and providing guarantees on the resulting closed-loop systems. We leverage *sums-of-squares (SOS) programming* to design these locally stabilizing controllers by explicitly attempting to minimize the size of the worst case reachable set of the closed-loop system subjected to bounded disturbances and uncertainty. The reachable sets associated with each trajectory in the library can be thought of as “funnels” that the system is guaranteed to remain within. The resulting *funnel library* is then used to *sequentially compose* motion plans at runtime while ensuring the safety of the robot. A major advantage of the work presented here is that by explicitly taking into account the effect of uncertainty, the robot can evaluate motion plans based on how vulnerable they are to disturbances. We demonstrate our method using thorough simulation experiments of a ground vehicle model navigating through cluttered environments and also present extensive hardware experiments validating the approach on a small fixed-wing airplane avoiding obstacles at high speed.

## 1 Introduction

Imagine an unmanned aerial vehicle (UAV) flying at high speeds through a cluttered environment in the presence of wind gusts, a legged robot traversing rough terrain, or a mobile robot grasping and manipulating previously unlocalized objects in the environment. Tasks such as these are characterized by three main challenges. First, the dynamics of the system are nonlinear, underactuated and subject to constraints on the input (e.g. torque limits). Second, there is a significant amount of uncertainty in the dynamics of the system due to disturbances and modeling error. Finally, the geometry of the environment that the robot is operating in is unknown until runtime, thus forcing the robot to plan *online* and in realtime.

Progress on such tasks has been spurred on by recent research in the field of motion planning. Planning algorithms like the Rapidly-exploring Randomized Tree (RRT) [Kuffner and Lavelle,

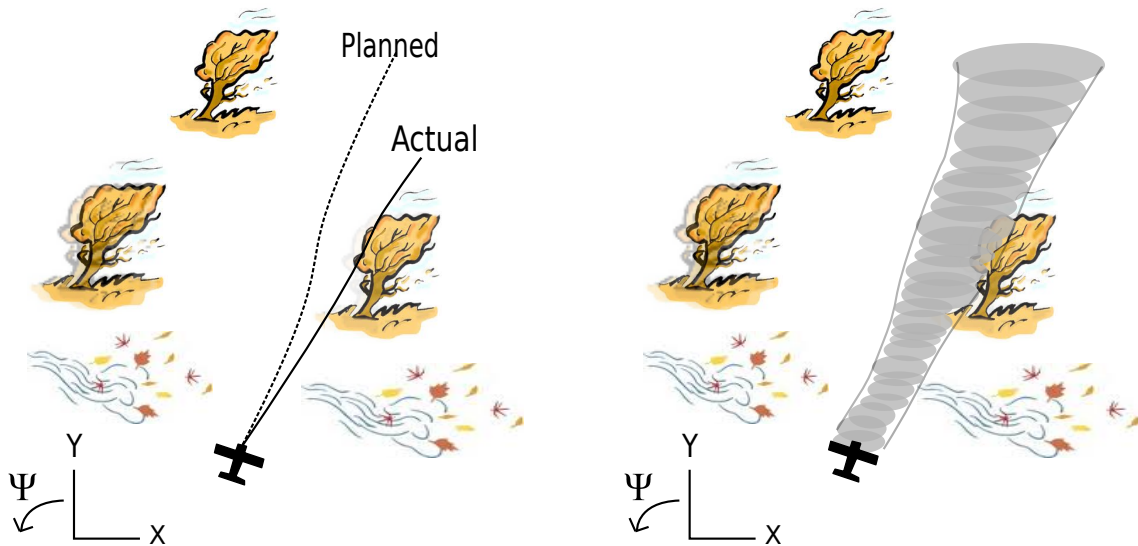
2000], RRT\* [Karaman and Frazzoli, 2011], and related methods based on trajectory libraries [Liu and Atkeson, 2009] [Frazzoli et al., 2005] [Stolle and Atkeson, 2006] can handle large state-space dimensions and complex differential constraints. These algorithms have been successfully demonstrated on a wide variety of hardware platforms [Shkolnik, 2010] [Sermanet et al., 2008]. However, a significant challenge these methods face is their inability to explicitly reason about uncertainty. Modeling errors, state uncertainty and disturbances can lead to failure if the system deviates from the planned nominal trajectories. This issue is sketched in Figure 1(a), where a UAV attempting to fly through a forest with a heavy cross-wind gets blown off its planned nominal trajectory and crashes into a tree.

Recently, planning algorithms which explicitly take into account feedback control have been proposed. The LQR-Trees algorithm [Tedrake et al., 2010] creates a tree of locally stabilizing controllers which can take any initial condition in some bounded region in state space to the desired goal. The approach leverages *sums-of-squares programming* (SOS) [Parrilo, 2000] for computing regions of finite time invariance for the locally stabilizing controllers. However, LQR-Trees lack the ability to handle scenarios in which the task and environment are unknown till runtime: the offline precomputation of the tree does not take into account potential runtime constraints like obstacles, and an online implementation of the algorithm is computationally infeasible.

In this paper, we address these problems by combining trajectory libraries, feedback control, and tools from Lyapunov theory and algorithmic algebra in order to perform robust online motion planning in the face of uncertainty. In particular, in the offline computation stage, we first design a finite library of open loop trajectories. For each trajectory in this library, we use *sums-of-squares programming* (SOS) to design a controller that explicitly attempts to minimize the size of the worst case reachable set of the system given a description of the uncertainty in the dynamics and bounded external disturbances. This control design procedure yields an outer approximation of the reachable set, which can be visualized as a “funnel” around the trajectory, that the closed-loop system is guaranteed to remain within. A cartoon of such a funnel is shown in Figure 1(b). Finally, we provide a way of *sequentially composing* these robust motion plans online in order to operate in a provably safe manner.

One of the most important advantages that our approach affords us is the ability to choose between the motion primitives in our library in a way that takes into account the dynamic effects of uncertainty. Imagine a UAV flying through a forest that has to choose between two motion primitives: a highly dynamic roll maneuver that avoids the trees in front of the UAV by a large margin or a maneuver that involves flying straight while avoiding the trees only by a small distance. An approach that neglects the effects of disturbances and uncertainty may prefer the former maneuver since it avoids the trees by a large margin and is therefore “safer”. However, a more careful consideration of the two maneuvers could lead to a different conclusion: the dynamic roll maneuver is far more susceptible to wind gusts and state uncertainty than the second one. Thus, it may actually be more robust to execute the second motion primitive. Further, it may be possible that neither maneuver is guaranteed to succeed and it is safer to abort the mission and simply transition to a hover mode. Our approach allows robots to make these critical decisions, which are essential if robots are to move out of labs and operate in real-world environments.

The outline of the paper is as follows. Section 2 discusses prior work; Section 3 provides a brief background on semidefinite and sums-of-squares (SOS) programming, which are used heavily throughout the paper; Section 4 shows how to use SOS programming to compute funnels; Section 5 introduces the notion of a funnel library; Section 6 describes our algorithm for using funnel libraries



(a) A plane deviating from its nominal planned trajectory due to a heavy cross-wind.

(b) The “funnel” of possible trajectories.

Figure 1: Not accounting for uncertainty while planning motions can lead to disastrous consequences.

for real-time robust planning in environments that have not been seen by the robot before; Section 7 presents extensive simulation results on a ground vehicle model and hardware results on the problem of high-speed obstacle avoidance for small fixed-wing airplane; and Section 8 concludes the paper.

## 2 Relevant Work

### 2.1 Motion Planning

Motion planning has been the subject of significant research in the last few decades and has enjoyed a large degree of success in recent years. Planning algorithms like the Rapidly-exploring Randomized Tree (RRT) [Kuffner and Lavelle, 2000], RRT\* [Karaman and Frazzoli, 2011], and related trajectory library approaches [Liu and Atkeson, 2009] [Frazzoli et al., 2005] [Stolle and Atkeson, 2006] can handle large state-space dimensions and complex differential constraints. These algorithms have been successfully demonstrated on a wide variety of hardware platforms [Shkolnik, 2010] [Sermanet et al., 2008]. However, an important challenge is their inability to explicitly reason about uncertainty and feedback. Modeling errors, state uncertainty and disturbances can lead to failure if the system deviates from the planned nominal trajectories.

The motion planning aspect of our approach draws inspiration from the vast body of work that is focused on computing motion primitives in the form of trajectory libraries. For example, trajectory libraries have been used in diverse applications such as humanoid balance control [Liu and Atkeson,

2009], autonomous ground vehicle navigation [Sermanet et al., 2008], and grasping [Berenson et al., 2007] [Dey et al., 2011]. The Maneuver Automaton [Frazzoli et al., 2005] attempts to capture the formal properties of trajectory libraries as a hybrid automaton, thus providing a unifying theoretical framework. Maneuver Automata have also been used for real-time motion planning with static and dynamic obstacles [Frazzoli et al., 2002]. Further theoretical investigations have focused on the offline generation of diverse but sparse trajectories that ensure the robot’s ability to perform the necessary tasks online in an efficient manner [Green and Kelly, 2007]. More recently, tools from sub-modular sequence optimization have been leveraged in the optimization of the sequence and content of trajectories evaluated online [Dey et al., 2011].

## 2.2 Feedback Motion Planning

Recently, planning algorithms which explicitly take into account feedback control have been proposed. The LQR-Trees algorithm [Tedrake et al., 2010] creates a tree of locally stabilizing controllers which can take any initial condition in some bounded region in state space to the desired goal. The approach leverages *sums-of-squares programming* (SOS) [Parrilo, 2000] for computing regions of finite time invariance for the locally stabilizing controllers. However, LQR-Trees lack the ability to handle scenarios in which the task and environment are unknown till runtime: the offline precomputation of the tree does not take into account potential runtime constraints like obstacles, and an online implementation of the algorithm is computationally infeasible.

## 2.3 Planning under Uncertainty and Robust Planning

The body of literature that deals with planning under uncertainty is also relevant to the work presented here [Bry and Roy, 2011] [Platt et al., 2010]. While these approaches generate motion plans that explicitly reason about the effect of uncertainty and disturbances on the behavior of the system, distributions over states (“belief states”) are typically approximated as Gaussians (however, see [Platt et al., 2012] for an exception to this) for computational efficiency and the true belief state is not tracked. Thus, in general, one does not have robustness guarantees. The approach we take here is to assume that disturbances/uncertainty are *bounded* and provide explicit bounds on the reachable set to facilitate safe operation of the system.

Robust motion planning has also been a very active area of research in the robotics community. Early work focused on the purely kinematic problem of planning paths through configuration space with “tubes” of specified radii around them such that all paths in the tube remain collision-free [Jacobs and Canny, 1990]. Recent work has focused on reasoning more explicitly about the manner in which disturbances and uncertainties influence the dynamics of the robot, and is closer in spirit to the work presented here. In particular, [Schouwenaars et al., 2003] approaches the problem through dynamic programming on a model with disturbances by making use of the Maneuver Automaton framework mentioned earlier. However, the work does not take into account obstacles in the environment and does not provide or make use of any explicit guarantees on allowed deviations from the planned trajectories in the Maneuver Automaton. Another approach that is closely related to ours is Model Predictive Control with Tubes [Mayne et al., 2005]. The idea is to solve the optimal control problem online with guaranteed “tubes” that the trajectories stay in. However, the method is limited to linear systems and convex constraints.



## 2.4 Reachable Set based Approaches

In [Gillula et al., 2010], the authors design motion primitives for making a quadrotor perform an autonomous backflip. Reachable sets for the primitives are computed via a Hamilton-Jacobi-Bellman differential game formulation [Mitchell et al., 2005]. However, a *predetermined* controller is employed for the reachability analysis instead of designing a controller that seeks to minimize the size of the reachable set (it is possible in principle to do this, but inconvenient in practice). More importantly, while their approach handles unsafe sets that the system is not allowed to enter, it is assumed that these sets are specified *a priori*. In this paper, we are concerned with scenarios in which unsafe sets (such as obstacles) are not specified until runtime and must thus be reasoned about *online*.

The approach that is perhaps most closely related to our work is the recent work presented in [Ny and Pappas, 2012]. The authors propose a randomized planning algorithm in the spirit of RRTs that explicitly reasons about disturbances and uncertainty. Specifications of input to output stability with respect to disturbances provide a parameterization of “tubes” (analogous to our “funnels”) that can be composed together to generate motion plans that are collision-free. The factors that distinguish the approach we present in this paper from the one proposed in [Ny and Pappas, 2012] are our focus on the *real-time* aspect of the problem and use of sums-of-squares programming as a way of computing reachable sets. In [Ny and Pappas, 2012], the focus is on generating safe motion plans when the obstacle positions are known *a priori*. Further, we provide a general technique for computing and explicitly minimizing the size of tubes.

## 2.5 Lyapunov Theory and SOS programming

A critical component of the work presented here is the computation of “funnels” for nonlinear systems via Lyapunov functions. This idea, along with the metaphor of a “funnel”, was introduced to the robotics community in [Burridge et al., 1999], where funnels were *sequentially composed* in order to produce dynamic behaviors in a robot. However, computational tools for automatically searching for Lyapunov functions were lacking until very recently. In recent years, sums-of-squares (SOS) programming has emerged as a way of checking the Lyapunov function conditions associated with each funnel [Parrilo, 2000]. The technique relies on the ability to check nonnegativity of multivariate polynomials by expressing them as a sum of squares of polynomials. This can be written as a semidefinite optimization program and is amenable to efficient computational algorithms such as interior point methods [Parrilo, 2000]. Assuming polynomial dynamics, one can check that a polynomial Lyapunov candidate,  $V(x)$ , satisfies  $V(x) > 0$  and  $\dot{V}(x) < 0$  in some region  $B_r$ . Importantly, the same idea can be used for designing controllers along time-indexed trajectories of a system that attempt to maximize the size of the set of initial conditions that are driven to a goal set [Tedrake et al., 2010]. In this paper, we will use a similar approach to compute controllers that explicitly minimize the size of reachable sets around trajectories. Thus, we are guaranteed that if the system starts off in the set of given initial conditions, it will remain in the computed “funnel” even if the model of the dynamics is uncertain and the system is subjected to bounded disturbances.

### 3 Background

In this section we provide a brief background on the key computational tools that will be employed throughout this paper.

#### 3.1 Semidefinite Programming (SDP)

Semidefinite programs (SDPs) form an important class of convex optimization problems. They are optimization problems over the space of symmetric positive semidefinite (psd) matrices. Recall that a  $n \times n$  symmetric matrix  $Q$  is positive semidefinite if  $x^T Q x \geq 0$ ,  $\forall x \in \mathbb{R}^n$ . Denoting the set of  $n \times n$  symmetric matrices as  $\mathbf{S}^n$ , a SDP in standard form is written as:

$$\begin{aligned} \min_{X \in \mathbf{S}^n} \quad & \langle C, X \rangle \\ \text{s.t.} \quad & \langle A_i, X \rangle = b_i \quad \forall i \in \{1, \dots, m\}, \\ & X \succeq 0, \end{aligned} \tag{1}$$

where  $C, A_i \in \mathbf{S}^n$  and  $\langle X, Y \rangle := \text{Tr}(X^T Y) = \sum_{i,j} X_{ij} Y_{ij}$ . In other words, a SDP involves minimizing a cost function that is linear in the elements of the decision matrix  $X$  subject to linear and positive semi definiteness constraints on  $X$ .

Semidefinite programming includes Linear Programming (LP), Quadratic Programming (QP) and Second-Order Cone Programming (SOCP) as special cases. As in these other cases, SDPs are amenable to efficient numerical solution via interior point methods. The interested reader may wish to consult [Vandenberghe and Boyd, 1996] and [Blekherman et al., 2013, Chapter 2] for a more thorough introduction to SDPs.

#### 3.2 Sums-of-Squares (SOS) Programming

An important application of SDPs is to check nonnegativity of polynomials. The decision problem associated with checking polynomial nonnegativity is NP-hard in general [Parrilo, 2000]. However, the problem of determining whether a polynomial is a sum-of-squares (SOS), which is a sufficient condition for nonnegativity, is amenable to efficient computation. A polynomial  $p$  in indeterminates<sup>1</sup>  $x_1, x_2, \dots, x_n$  is SOS if it can be written as  $p(x) = \sum_{i=1}^m q_i^2(x)$  for a set of polynomials  $\{q_i\}_{i=1}^m$ . This condition is *equivalent* to the existence of a psd matrix  $Q$  that satisfies:

$$p(x) = v(x)^T Q v(x), \quad \forall x \in \mathbb{R}^n, \tag{2}$$

where  $v(x)$  is the vector of all monomials with degree less than or equal to half the degree of  $p$  [Parrilo, 2000]. Note that the equality constraint (2) imposes linear constraints on the elements of the matrix  $Q$  that come from matching coefficients of the polynomials on the left and right hand sides. Thus, semidefinite programming can be used to certify that a polynomial is a sum of squares. Indeed, by allowing the coefficients of the polynomial  $p$  to be decision variables, we can solve optimization problems over the space of SOS polynomials of some fixed degree. Such

---

<sup>1</sup>Throughout this paper, the variables  $x$  that a polynomial  $p(x)$  depend on will be referred to as “indeterminates”. This is to distinguish these variables from *decision variables* in our optimization problems, which will typically be the coefficients of the polynomial.

optimization problems are referred to as sums-of-squares (SOS) programs. The interested reader is referred to [Blekherman et al., 2013, Chapters 3,4] for a more thorough introduction to SOS programming.

In addition to being able to prove global nonnegativity of polynomials, the SOS programming approach can also be used to demonstrate nonnegativity of polynomials on basic semialgebraic sets (i.e., sets described by a finite number of polynomial inequalities and equalities). Suppose we are given a set  $\mathcal{B}$ :

$$\mathcal{B} = \{x \in \mathbb{R}^n \mid g_{eq,i}(x) = 0, g_{ineq,j}(x) \geq 0\}, \quad (3)$$

where  $g_{eq,i}$  and  $g_{ineq,j}$  are polynomials for  $i \in \{1, \dots, N_{eq}\}, j \in \{1, \dots, N_{ineq}\}$ . We are interested in showing that a polynomial  $p$  is nonnegative on the set  $\mathcal{B}$ :

$$x \in \mathcal{B} \implies p(x) \geq 0. \quad (4)$$

We can write the following SOS constraints in order to impose (4):

$$q(x) := p(x) - \overbrace{\sum_{i=1}^{N_{eq}} L_{eq,i}(x)g_{eq,i}(x) - \sum_{j=1}^{N_{ineq}} L_{ineq,j}(x)g_{ineq,j}(x)}^{r(x)} \text{ is SOS} \quad (5)$$

$$L_{ineq,j}(x) \text{ is SOS}, \forall j \in \{1, \dots, N_{ineq}\}. \quad (6)$$

Here, the polynomials  $L_{eq,i}$  and  $L_{ineq,j}$  are “multiplier” polynomials analogous to Lagrange multipliers in constrained optimization. In order to see that (5) and (6) are sufficient conditions for (4), note that when a point  $x$  satisfies  $g_{eq,i}(x) = 0$  and  $g_{ineq,j}(x) \geq 0$  for  $i \in \{1, \dots, N_{eq}\}, j \in \{1, \dots, N_{ineq}\}$  (i.e., when  $x \in \mathcal{B}$ ) then the term  $r(x)$  is non-positive. Hence, for  $q(x)$  to be nonnegative (which must be the case since  $q$  is SOS),  $p(x)$  must be nonnegative. Thus, we have the desired implication in (4). This process for using multipliers to impose nonnegativity constraints on sets is known as the generalized S-procedure [Parrilo, 2000] and will be used extensively in Section 4 for computing funnels.

## 4 Computing Funnels

In this section we describe how the tools from Section 3 can be used to compute outer approximations of reachable sets (“funnels”) around trajectories of a nonlinear system. The approach in Section 4.1 is based on [Tobenkin et al., 2011, Tedrake et al., 2010] while Sections 4.2.1 and 4.2.2 are based on [Majumdar and Tedrake, 2012] and [Majumdar et al., 2013] respectively. In contrast to this prior work however, we consider the problem of computing outer approximations of forwards reachable sets as opposed to inner approximations of backwards reachable sets. This leads to a few subtle differences in the cost functions of our optimization problems.

Consider the following dynamical system:

$$\dot{x} = f(x(t), u(t)), \quad (7)$$

where  $x(t) \in \mathbb{R}^n$  is the state of the system at time  $t$  and  $u(t) \in \mathbb{R}^m$  is the control input. Let  $x_0 : [0, T] \rightarrow \mathbb{R}^n$  be the nominal trajectory that we would like the system to follow and  $u_0 : [0, T] \rightarrow \mathbb{R}^m$

be the nominal open-loop control input. Defining new coordinates  $\bar{x} = x - x_0(t)$  and  $\bar{u} = u - u_0(t)$ , we can rewrite the dynamics (7) in these variables as:

$$\dot{\bar{x}} = \dot{x} - \dot{x}_0 = f(x_0(t) + \bar{x}(t), u_0(t) + \bar{u}(t)) - \dot{x}_0. \quad (8)$$

We will first consider the problem of computing funnels for a closed-loop system subject to no uncertainty. To this end, we assume that we are given a feedback controller  $\bar{u}_f(t, \bar{x})$  that corrects for deviations around the nominal trajectory (we will consider the problem of designing feedback controllers later in this section). We can then write the closed-loop dynamics of the system as:

$$\dot{\bar{x}} = f_{cl}(t, \bar{x}(t)). \quad (9)$$

Given a set of initial conditions  $\mathcal{X}_0 \subset \mathbb{R}^n$  with  $x_0(0) \in \mathcal{X}_0$ , our goal is to find a tight outer approximation of the set of states the system may evolve to at time  $t \in [0, T]$ . In particular, we are concerned with finding sets  $F(t) \subset \mathbb{R}^n$  such that:

$$\bar{x}(0) \in \mathcal{X}_0 \implies \bar{x}(t) \in F(t), \forall t \in [0, T]. \quad (10)$$

**Definition 1.** A funnel associated with a closed-loop dynamical system  $\dot{\bar{x}} = f_{cl}(t, \bar{x}(t))$  is a map  $F : [0, T] \rightarrow \mathcal{P}(\mathbb{R}^n)$  from the time-interval  $[0, T]$  to the power set (i.e., the set of subsets) of  $\mathbb{R}^n$  such that the sets  $F(t)$  satisfy the condition (10) above.

We will parameterize the sets  $F(t)$  as sub-level sets of nonnegative time-varying functions  $V : [0, T] \times \mathbb{R}^n \rightarrow \mathbb{R}^+$ :

$$F(t) = \{\bar{x}(t) \in \mathbb{R}^n | V(t, \bar{x}(t)) \leq \rho(t)\}. \quad (11)$$

Letting  $\mathcal{X}_0 \subset F(0, \bar{x})$ , the following constraint is a sufficient condition for (10):

$$V(t, \bar{x}) = \rho(t) \implies \dot{V}(t, \bar{x}) < \dot{\rho}(t), \forall t \in [0, T]. \quad (12)$$

Here,  $\dot{V}$  is computed as:

$$\dot{V}(t, \bar{x}) = \frac{\partial V(t, \bar{x})}{\partial \bar{x}} f_{cl}(t, \bar{x}) + \frac{\partial V(t, \bar{x})}{\partial t}. \quad (13)$$

Intuitively, the constraint (12) says that on the boundary of the funnel (i.e., when  $V(t, \bar{x}) = \rho(t)$ ), the function  $V$  grows slower than  $\rho$ . Hence, states on the boundary of the funnel remain within the funnel. This intuition is formalized in [Tadrake et al., 2010, Tobenkin et al., 2011].

While *any* function that satisfies (12) provides us with a valid funnel, we are interested in finding *tight* outer approximations of the reachable set. A natural cost function for encouraging tightness is the volume of the sets  $F(t)$ . Combining this cost function with our constraints, we obtain the following optimization problem:

$$\begin{aligned} \inf_{V, \rho} \quad & \int_0^T \text{vol}(F(t)) \, dt \\ \text{s.t.} \quad & V(t, \bar{x}) = \rho(t) \implies \dot{V}(t, \bar{x}) < \dot{\rho}(t), \forall t \in [0, T], \\ & \mathcal{X}_0 \subset F(0, \bar{x}). \end{aligned} \quad (14)$$

#### 4.1 Numerical implementation using SOS programming

Since the optimization problem (14) involves searching over spaces of functions, it is infinite dimensional and hence not directly amenable to numerical computation. However, we can use the SOS programming approach described in Section 3 to obtain finite dimensional optimization problems in the form of semidefinite programs (SDPs). We first concentrate on implementing the constraints in (14). We will assume that the initial condition set  $\mathcal{X}_0$  is a semi-algebraic set (i.e., described in terms of polynomial inequalities):

$$\mathcal{X}_0 = \{\bar{x} \in \mathbb{R}^n \mid g_{0,i}(\bar{x}) \geq 0, \forall i = 1, \dots, N_0\}. \quad (15)$$

Then the constraints in (14) can be written as:

$$V(t, \bar{x}) = \rho(t) \implies \rho(t) - \dot{V}(t, \bar{x}) > 0 \quad (16)$$

$$g_{0,i}(\bar{x}) \geq 0 \forall i \in \{1, \dots, N_0\} \implies \rho(0) - V(0, \bar{x}) \geq 0. \quad (17)$$

If we restrict ourselves to polynomial dynamics and polynomial functions  $V$  and  $\rho$ , these constraints are precisely in the form of (4) in Section 3.2. We can thus apply the procedure described in Section 3.2 and arrive at the following sufficient conditions for (16) and (17):

$$\dot{\rho}(t) - \dot{V}(t, \bar{x}) - L(t, \bar{x})[V(t, \bar{x}) - \rho(t)] - L_t(t, \bar{x})[t(T - t)] \text{ is SOS}, \quad (18)$$

$$\rho(0) - V(0, \bar{x}) - \sum_i^{N_0} L_{0,i}(\bar{x})g_{0,i}(\bar{x}) \text{ is SOS}, \quad (19)$$

$$L_t(t, \bar{x}), L_{0,i}(\bar{x}) \text{ are SOS}, \forall i \in \{1, \dots, N_0\}. \quad (20)$$

As in Section 3.2, the polynomials  $L, L_t$  and  $L_{0,i}$  are “multiplier” polynomials whose coefficients are decision variables.

Next, we focus on approximating the cost function in (14) using semidefinite programming. This can be achieved by sampling in time and replacing the integral with the finite sum  $\sum_{k=1}^N \text{vol}(F(t_k))$ . In the special case where the function  $V$  is quadratic in  $\bar{x}$ :

$$V(t_k, \bar{x}) = \bar{x}^T S_k \bar{x}, \quad S_k \succeq 0, \quad (21)$$

the set  $F(t_k)$  is an ellipsoid and we can use semidefinite programming to directly minimize the volume by maximizing the determinant of  $S_k$  (recall that the volume of the ellipsoid  $F(t_k)$  is a monotonically decreasing function of the determinant of  $S_k$ ). Note that while the problem of maximizing the determinant of a psd matrix is not directly a problem of the form (1), it can be transformed into such a form [Ben-Tal and Nemirovski, 2001, Chapter3]. In the more general case, we can minimize an upper bound on the cost function  $\sum_{k=1}^N \text{vol}(F(t_k))$  by introducing ellipsoids  $\mathcal{E}(t_k)$ :

$$\mathcal{E}(t_k) = \{\bar{x} \in \mathbb{R}^n \mid \bar{x}^T S_k \bar{x} \leq 1, \quad S_k \succeq 0\} \quad (22)$$

such that  $F(t_k) \subset \mathcal{E}(t_k)$  and minimizing  $\sum_{k=1}^N \text{vol}(\mathcal{E}(t_k))$ . The containment constraint can be equivalently expressed as the constraint:

$$V(t_k, \bar{x}) \leq \rho(t_k) \implies \bar{x}^T S_k \bar{x} \leq 1, \quad (23)$$

and can thus be imposed using SOS constraints:

$$1 - \bar{x}^T S_k \bar{x} - L_{\mathcal{E},k}(\bar{x})[\rho(t_k) - V(t_k, \bar{x})] \text{ is SOS,} \quad (24)$$

$$L_{\mathcal{E},k}(\bar{x}) \text{ is SOS.} \quad (25)$$

Combining our cost function with the constraints (18) - (20), we obtain the following optimization problem:

$$\inf_{V, \rho, L, L_t, L_{0,i}, S_k, L_{\mathcal{E},k}} \sum_{k=1}^N \text{vol}(\mathcal{E}(t_k)) = \sum_{k=1}^N \text{vol}(\{\bar{x} | \bar{x}^T S_k \bar{x} \leq 1\}) \quad (26)$$

$$\text{s.t.} \quad \dot{\rho}(t) - \dot{V}(t, \bar{x}) - L(t, \bar{x})[V(t, \bar{x}) - \rho(t)] - L_t(t, \bar{x})[t(T - t)] \text{ is SOS,} \quad (27)$$

$$\rho(0) - V(0, \bar{x}) - \sum_i^{N_0} L_{0,i}(\bar{x}) g_{0,i}(\bar{x}) \text{ is SOS,}$$

$$1 - \bar{x}^T S_k \bar{x} - L_{\mathcal{E},k}(\bar{x})[\rho(t_k) - V(t_k, \bar{x})] \text{ is SOS,} \quad \forall k \in \{1, \dots, N\},$$

$$S_k \succeq 0, \quad \forall k \in \{1, \dots, N\},$$

$$L_t(t, \bar{x}), L_{0,i}(\bar{x}), L_{\mathcal{E},k}(\bar{x}) \text{ are SOS,} \quad \forall i \in \{1, \dots, N_0\}, \forall k \in \{1, \dots, N\}.$$

While this optimization problem is finite dimensional, it is non-convex in general since the first constraints are *bilinear* in the decision variables (e.g., the coefficients of the polynomials  $L$  and  $V$  are multiplied together in the first constraint). To apply SOS programming, we require the constraints to be linear in the coefficients of the polynomials we are optimizing. However, note that when  $V$  and  $\rho$  are fixed, the constraints are linear in the other decision variables. Similarly, when the multipliers  $L$  and  $L_{\mathcal{E},k}$  are fixed, the constraints are linear in the remaining decision variables. Thus, we can efficiently perform this optimization by alternating between the two sets of decision variables  $(L, L_t, L_{0,i}, S_k, L_{\mathcal{E},k})$  and  $(V, \rho, L_t, L_{0,i}, S_k)$ . In each step of the alternation, we can optimize our cost function  $\sum_{k=1}^N \text{vol}(\mathcal{E}(t_k))$ . These alternations are summarized in Algorithm 1. Note that the algorithm requires an initialization for  $V$  and  $\rho$ . We will discuss how to obtain these in Section 4.3.

**Remark 1.** *It is easy to see that Algorithm 1 converges (though not necessarily to an optimal solution). Each iteration of the alternations is guaranteed to achieve a cost function that is at least as good as the previous iteration (since the solution from the previous iteration is a valid one). Hence, the sequence of optimal values in each iteration form a monotonically non-increasing sequence. Combined with the fact that the cost function is bounded below by 0, we conclude that this sequence converges and hence that Algorithm 1 terminates.*

#### 4.1.1 Approximation via time-sampling

As observed in [Tobenkin et al., 2011] in practice it is often the case that the nominal trajectory  $x_0 : [0, T] \rightarrow \mathbb{R}^n$  is difficult to approximate with a low degree polynomial in time. This can lead to the constraint (27) in the problem (26) having a high degree polynomial dependence on  $t$ . Thus it is often useful to implement an approximation of the optimization problem (26) where the condition (16) is checked only at a finite number of sample points  $t_k \in [0, T]$ ,  $k \in \{1, \dots, N\}$ . We can use a piecewise linear parameterization of  $\rho$  and can thus compute:

$$\dot{\rho}(t_k) = \frac{\rho(t_{k+1}) - \rho(t_k)}{t_{k+1} - t_k}. \quad (28)$$

---

**Algorithm 1** Funnel Computation

---

```

1: Initialize  $V$  and  $\rho$ .
2:  $cost_{prev} = \infty$ ;
3: converged = false;
4: while  $\neg$ converged do
5:   STEP 1 : Minimize  $\sum_{k=1}^N vol(\mathcal{E}(t_k))$  by searching for multiplier polynomials  $(L, L_t, L_{0,i}, L_{\mathcal{E},k})$ 
      and  $S_k$  while fixing  $V$  and  $\rho$ .
6:   STEP 2 : Minimize  $\sum_{k=1}^N vol(\mathcal{E}(t_k))$  by searching for  $(V, \rho, L_t, L_{0,i}, S_k)$  while fixing  $L$  and
       $L_{\mathcal{E},k}$ .
7:    $cost = \sum_{k=1}^N vol(\mathcal{E}(t_k))$ ;
8:   if  $\frac{cost_{prev} - cost}{cost_{prev}} < \epsilon$  then
9:     converged = true;
10:  end if
11:   $cost_{prev} = cost$ ;
12: end while

```

---

Similarly we can parameterize the function  $V$  by polynomials  $V_k(\bar{x})$  at each time sample and compute:

$$\frac{\partial V(t, \bar{x})}{\partial t} \approx \frac{V_{k+1}(\bar{x}) - V_k(\bar{x})}{t_{k+1} - t_k}. \quad (29)$$

We can then write the following modified version of the problem (26):

$$\begin{aligned}
\inf_{V_k, \rho, L_k, L_{0,i}, S_k, L_{\mathcal{E},k}} \quad & \sum_{k=1}^N vol(\mathcal{E}(t_k)) = \sum_{k=1}^N vol(\{\bar{x} | \bar{x}^T S_k \bar{x} \leq 1\}) \\
\text{s.t.} \quad & \dot{\rho}(t_k) - \dot{V}_k(\bar{x}) - L_k(\bar{x})[V_k(\bar{x}) - \rho(t_k)], \quad \forall k \in \{1, \dots, N\}, \\
& \rho(t_1) - V_1(\bar{x}) - \sum_i^{N_0} L_{0,i}(\bar{x}) g_{0,i}(\bar{x}) \text{ is SOS}, \\
& 1 - \bar{x}^T S_k \bar{x} - L_{\mathcal{E},k}(\bar{x})[\rho(t_k) - V_k(\bar{x})] \text{ is SOS}, \quad \forall k \in \{1, \dots, N\}, \\
& S_k \succeq 0, \quad \forall k \in \{1, \dots, N\}, \\
& L_{0,i}(\bar{x}), L_{\mathcal{E},k}(\bar{x}) \text{ are SOS}, \quad \forall i \in \{1, \dots, N_0\}, \forall k \in \{1, \dots, N\}.
\end{aligned} \quad (30)$$

This program does not have any algebraic dependence on the variable  $t$  and can thus provide significant computational gains over (26). However, it does not provide an exact funnel certificate. One would hope that with a sufficiently fine sampling in time, one would recover exactness. Partial results in this direction are provided in [Tobenkin et al., 2011] along with numerical examples showing that the loss of accuracy from the sampling approximation can be quite small in practice.

The problem (30) is again bilinear in the decision variables. It is linear in the two sets of decision variables  $(L_k, L_{0,i}, S_k, L_{\mathcal{E},k})$  and  $(V_k, \rho, L_{0,i}, S_k)$ . Thus, Algorithm 1 can be applied directly to (30) with the minor modification that  $V$  and  $\rho$  are replaced by their time-sampled counterparts and the multipliers  $(L, L_t)$  are replaced by the multipliers  $L_k$ .

## 4.2 Extensions to the basic algorithm

Next we describe several extensions to the basic framework for computing funnels described in Section 4.1. Section 4.2.1 discusses the scenario in which the dynamics of the system are subject to bounded disturbances/uncertainty, Section 4.2.2 considers the problem of synthesizing feedback controllers that explicitly attempt to minimize the size of the funnel, Section 4.2.3 demonstrates how to handle input saturations, and Section 4.2.4 considers a generalization of the cost function.

### 4.2.1 Uncertainty in the dynamics

Suppose that the dynamics of the system are subject to an uncertainty term  $w(t) \in \mathbb{R}^d$  that models external disturbances or parametric model uncertainties. The closed-loop dynamics (9) can then be modified to capture this uncertainty:

$$\dot{\bar{x}} = f_{cl}(t, \bar{x}(t), w(t)). \quad (31)$$

We will assume that the dynamics  $f_{cl}$  depend polynomially on  $w$ . Given an initial condition set  $\mathcal{X}_0 \subset \mathbb{R}^n$  as before, our goal is to find sets  $F(t)$  such that  $x(t)$  is guaranteed to be in  $F(t)$  for any valid disturbance profile:

$$\bar{x}(0) \in \mathcal{X}_0 \implies \bar{x}(t) \in F(t), \forall t \in [0, T], \forall w : [0, T] \rightarrow \mathcal{W}. \quad (32)$$

Parameterizing the sets  $F(t)$  as sub-level sets of nonnegative time-varying functions  $V : [0, T] \times \mathbb{R}^n \rightarrow \mathbb{R}^+$  as before, the following condition is sufficient to ensure (32):

$$V(t, \bar{x}) = \rho(t) \implies \dot{V}(t, \bar{x}, w) < \dot{\rho}(t), \forall t \in [0, T], \forall w(t) \in \mathcal{W}, \quad (33)$$

where  $\dot{V}$  is computed as:

$$\dot{V}(t, \bar{x}, w) = \frac{\partial V(t, \bar{x})}{\partial \bar{x}} f_{cl}(t, \bar{x}, w) + \frac{\partial V(t, \bar{x})}{\partial t}. \quad (34)$$

This is almost identical to the condition (12), with the exception that the function  $V$  is required to decrease on the boundary of the funnel for every choice of disturbance. Assuming that the set  $\mathcal{W}$  is a semi-algebraic set  $\mathcal{W} = \{w \in \mathbb{R}^d \mid g_{w,j}(w) \geq 0, \forall j = 1, \dots, N_w\}$ , the optimization problem (26) is then easily modified by replacing condition (27) with the following constraints:

$$\begin{aligned} \dot{\rho}(t) - \dot{V}(t, \bar{x}, w) - L(t, \bar{x}, w)[V(t, \bar{x}) - \rho(t)] - L_t(t, \bar{x}, w)[t(T - t)] - \sum_{j=1}^{N_w} L_{w,j}(t, \bar{x}, w)g_{w,j}(w) \text{ is SOS,} \\ L_{w,j}(t, \bar{x}, w) \text{ is SOS, } \forall j = \{1, \dots, N_w\}. \end{aligned} \quad (35)$$

These SOS constraints now involve polynomials in the indeterminates  $t, \bar{x}$  and  $w$ . Since these constraints are linear in the coefficients of the newly introduced multipliers  $L_{w,j}$ , Algorithm 1 can be directly applied to the modified optimization problem by adding  $L_{w,j}$  to the list of polynomials to be searched for in both Step 1 and Step 2 of the iterations. Similarly, the time-sampled approximation described in Section 4.1.1 can also be applied to (35).



### 4.2.2 Feedback control synthesis

So far we have assumed that we have been provided with a feedback controller that corrects for deviations around the nominal trajectory. We now consider the problem of *optimizing* the feedback controller in order to minimize the size of the funnel. We will assume that the system is control affine:

$$\dot{x} = f(x(t)) + g(x(t))u(t), \quad (36)$$

and parameterize the control policy as a polynomial  $\bar{u}_f(t, \bar{x})$ . We can thus write the dynamics in the  $\bar{x}$  coordinates as:

$$\dot{\bar{x}} = f(x_0(t) + \bar{x}(t)) + g(x(t))[u_0(t) + \bar{u}_f(t, \bar{x})] - \dot{x}_0. \quad (37)$$

The feedback controller can then be optimized by adding the coefficients of the polynomial  $\bar{u}_f(t, \bar{x})$  to the set of decision variables in the optimization problem (26) while keeping all the constraints unchanged. Note that  $\bar{u}_f$  appears in the constraints only through  $\dot{V}$ , which is now bilinear in the coefficients of  $V$  and  $\bar{u}_f$  since:

$$\dot{V}(t, \bar{x}) = \frac{\partial V(t, \bar{x})}{\partial \bar{x}} \dot{\bar{x}} + \frac{\partial V(t, \bar{x})}{\partial t}. \quad (38)$$

With the (coefficients of) the feedback controller  $\bar{u}_f$  as part of the optimization problem, note that the constraints of the problem (26) are now bilinear in the two sets of decision variables  $(L, L_t, L_{0,i}, S_k, L_{\mathcal{E},k}, \bar{u}_f)$  and  $(V, \rho, L_t, L_{0,i}, S_k)$ . Thus, in principle we could use a bilinear alternation scheme similar to the one in Algorithm 1 and alternatively optimize these two sets of decision variables. However, in this case we would not be searching for a controller that explicitly seeks to minimize the size of the funnel (since the controller would not be searched for at the same time as  $V$  or  $\rho$ , which define the funnel). To get around this issue, we add another step in each iteration where we optimize our cost function  $\sum_{k=1}^N \text{vol}(\mathcal{E}(t_k))$  by searching for  $(\bar{u}_f, \rho, L_t, L_{0,i}, S_k)$  while keeping  $(V, L, L_{\mathcal{E},k})$  fixed. This allows us to search for  $\bar{u}_f$  and  $\rho$  at the same time, which can significantly improve the quality of the controllers and funnels we obtain. These steps are summarized in Algorithm 2. By a reasoning identical to the one in Remark 1 it is easy to see that the sequence of optimal values produced by Algorithm 2 converges.

We note that the approach for taking into account uncertainty described in Section 4.2.1 can easily be incorporated into Algorithm 2. Similarly, by parameterizing the controller  $\bar{u}_f$  as polynomials  $u_{f,k}(\bar{x})$  at the times  $t_k$ , we can also apply the time-sampled approximation described in Section 4.1.1.

### 4.2.3 Actuator saturations

#### A. Approach 1

Our approach also allows us to incorporate actuator limits into the verification procedure. Although we examine the single-input case in this section, this framework is easily extended to handle multiple inputs. Let the control input  $u(t)$  at time  $t$  be mapped through the following control saturation function:

$$s(u(t)) = \begin{cases} u_{max} & \text{if } u(t) \geq u_{max} \\ u_{min} & \text{if } u(t) \leq u_{min} \\ u(t) & \text{o.w.} \end{cases}$$

---

**Algorithm 2** Feedback Control Synthesis

---

```
1: Initialize  $V$  and  $\rho$ .
2:  $cost_{prev} = \infty$ ;
3: converged = false;
4: while  $\neg$ converged do
5:   STEP 1 : Minimize  $\sum_{k=1}^N vol(\mathcal{E}(t_k))$  by searching for controller  $\bar{u}_f$  and  $(L, L_t, L_{0,i}, L_{\mathcal{E},k}, S_k)$ 
     while fixing  $V$  and  $\rho$ .
6:   STEP 2 : Minimize  $\sum_{k=1}^N vol(\mathcal{E}(t_k))$  by searching for controller  $\bar{u}_f$  and  $(\rho, L_t, L_{0,i}, S_k)$  while
     fixing  $(V, L, L_{\mathcal{E},k})$ .
7:   STEP 3 : Minimize  $\sum_{k=1}^N vol(\mathcal{E}(t_k))$  by searching for  $(V, \rho, L_t, L_{0,i}, S_k)$  while fixing
      $(L, L_{\mathcal{E},k}, \bar{u}_f)$ .
8:    $cost = \sum_{k=1}^N vol(\mathcal{E}(t_k))$ ;
9:   if  $\frac{cost_{prev} - cost}{cost_{prev}} < \epsilon$  then
10:     converged = true;
11:   end if
12:    $cost_{prev} = cost$ ;
13: end while
```

---

Then, in a manner similar to [Tedrake et al., 2010], a piecewise analysis of  $\dot{V}(t, \bar{x})$  can be used to check the Lyapunov conditions are satisfied even when the control input saturates. Defining:

$$\dot{V}_{min}(t, \bar{x}) := \frac{\partial V(t, \bar{x})}{\partial \bar{x}} \left( f(x_0 + \bar{x}) + g(x_0 + \bar{x})u_{min} \right) + \frac{\partial V(t, \bar{x})}{\partial t}, \quad (39)$$

$$\dot{V}_{max}(t, \bar{x}) := \frac{\partial V(t, \bar{x})}{\partial \bar{x}} \left( f(x_0 + \bar{x}) + g(x_0 + \bar{x})u_{max} \right) + \frac{\partial V(t, \bar{x})}{\partial t}, \quad (40)$$

we must check the following conditions:

$$u_0(t) + \bar{u}_f(t, \bar{x}) \leq u_{min}, \quad V(t, \bar{x}) = \rho(t) \implies \dot{V}_{min}(t, \bar{x}) < \dot{\rho}(t), \quad (41)$$

$$u_0(t) + \bar{u}_f(t, \bar{x}) \geq u_{max}, \quad V(t, \bar{x}) = \rho(t) \implies \dot{V}_{min}(t, \bar{x}) < \dot{\rho}(t), \quad (42)$$

$$u_{min} \leq u_0(t) + \bar{u}_f(t, \bar{x}) \leq u_{max}, \quad V(t, \bar{x}) = \rho(t) \implies \dot{V}(t, \bar{x}) < \dot{\rho}(t), \quad (43)$$

where  $u_0$  is the open-loop control input and  $\bar{u}_f$  is the feedback controller as before. These conditions can be enforced by adding additional multipliers to the optimization program (26) or its time-sampled counterpart (30).

## B. Approach 2

Although one can handle multiple inputs via the above method, the number of SOS conditions grows exponentially with the number of inputs ( $3^m$  conditions for  $\dot{V}$  are needed in general to handle all possible combinations of input saturations). Thus, for systems with a large number of inputs, an alternative formulation was proposed in [Majumdar et al., 2013] that avoids this exponential growth in the size of the SOS program at the cost of adding conservativeness to the size of the funnel. Given limits on the control vector  $u \in \mathbb{R}^m$  of the form  $u_{min} < u < u_{max}$ , we can ask to satisfy:

$$\bar{x} \in F(t) \implies u_{min} < u_0(t) + \bar{u}_f(t, \bar{x}) < u_{max}, \quad \forall t \in [0, T]. \quad (44)$$

This constraint implies that the applied control input remains within the specified bounds inside the verified funnel (a conservative condition). The number of extra constraints grows linearly with the number of inputs (since we have one new condition for every input), thus leading to smaller optimization problems.

#### 4.2.4 A more general cost function

We end our discussion of extensions to the basic algorithm for computing funnels presented in Section 4.1 by considering a generalization of the cost function (volume of the funnel) we have used so far. In particular, it is sometimes useful to minimize the volume of the funnel *projected* onto a subspace of the state space. Suppose this projection map is given by  $\pi : \mathbb{R}^n \rightarrow \mathbb{R}^{n_p}$  with a corresponding  $n_p \times n$  projection matrix  $P$ . For an ellipsoid  $\mathcal{E} = \{\bar{x} \in \mathbb{R}^n \mid \bar{x}^T S_k \bar{x} \leq 1\}$ , the projected set  $\pi(\mathcal{E})$  is also an ellipsoid  $\mathcal{E}_p = \{\bar{x} \in \mathbb{R}^{n_p} \mid \bar{x}^T S_k^{(p)} \bar{x} \leq 1\}$  with:

$$S_k^{(p)} = (P S_k^{-1} P^T)^{-1}. \quad (45)$$

Recall that the ability to minimize the volume of the ellipsoid  $\mathcal{E}$  using SDP relied on being able to maximize the determinant of  $S_k$ . In order to minimize the volume of  $\mathcal{E}_p$ , we would have to maximize  $\det(S_k^{(p)})$ , which is a complicated (i.e. nonlinear) function of  $S_k$ . Hence, in each iteration of Algorithm 1 we linearize the function  $\det(S_k^{(p)})$  with respect to  $S_k$  at the solution of  $S_k$  from the previous iteration and maximize this linearization instead. The linearization of  $\det(S_k^{(p)})$  with respect to  $S_k$  at a nominal value  $S_{k,0}$  can be explicitly computed as:

$$\text{Tr}\left(P^T (P S_{k,0}^{-1} P^T)^{-1} P S_{k,0}^{-1} S_k S_{k,0}^{-1}\right), \quad (46)$$

where  $\text{Tr}$  refers to the trace of the matrix.

### 4.3 Implementation details

We end this section on computing funnels by discussing a few important implementation details.

#### 4.3.1 Trajectory generation

An important step that is necessary for the success of our approach to computing funnels is the generation of a dynamically feasible open-loop control input  $u_0 : [0, T] \mapsto \mathbb{R}^m$  and corresponding nominal trajectory  $x_0 : [0, T] \mapsto \mathbb{R}^n$ . A method that has been shown to work well in practice and scale to high dimensions is the direct collocation trajectory optimization method [Betts, 2001]. While this is the approach we use for the results in Section 7, other methods like the Rapidly Exploring Randomized Tree (RRT) or its asymptotically optimal version, RRT\* can be used too [Kuffner and Lavalley, 2000, Karaman and Frazzoli, 2011].

#### 4.3.2 Initializing $V$ and $\rho$

Algorithms 1 and 2 require an initial guess for the functions  $V$  and  $\rho$ . In [Tedrake et al., 2010], the authors use the Lyapunov function candidate associated with a time-varying LQR controller. The control law is obtained by solving a Riccati differential equation:

$$-\dot{S}(t) = Q - S(t)B(t)R^{-1}B^T S(t) + S(t)A(t) + A(t)^T S(t) \quad (47)$$

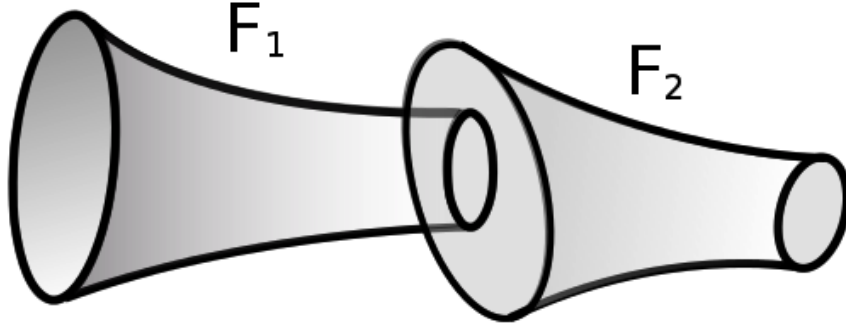


Figure 2: The ordered pair of funnels  $(F_1, F_2)$  is sequentially composable. The outlet of  $F_1$  is contained within the inlet of  $F_2$ , i.e.,  $F_1(T_1) \subset F_2(0)$ .

with final value conditions  $S(t) = S_f$ . Here  $A(t)$  and  $B(t)$  describe the time-varying linearization of the dynamics about the nominal trajectory  $x_0$ . The matrices  $Q$  and  $R$  are positive-definite cost-matrices. The function:

$$V_{guess}(t, \bar{x}) = (x - x_0(t))^T S(t) (x - x_0(t)) = \bar{x}^T S(t) \bar{x} \quad (48)$$

is our initial Lyapunov candidate. Setting  $\rho$  to a quickly increasing function such as an exponential is typically sufficient to obtain a feasible initialization.

## 5 Funnel Libraries

### 5.1 Sequential composition

One can think of funnels computed using the machinery described in Section 4 as *robust* motion primitives (the robustness is to initial conditions and uncertainty in the dynamics). While we could define a *funnel library* simply as a collection  $\mathcal{F}$  of funnels and associated feedback controllers, it will be fruitful to associate some additional structure with  $\mathcal{F}$ . In particular, it is useful to know how funnels can be *sequenced* together to form composite robust motion plans. In order to consider this more formally, we will first introduce the notion of *sequential composition* of funnels defined in [Burridge et al., 1999].

**Definition 2.** [Burridge et al., 1999] *An ordered pair  $(F_1, F_2)$  of funnels  $F_1 : [0, T_1] \rightarrow \mathcal{P}(\mathbb{R}^n)$  and  $F_2 : [0, T_2] \rightarrow \mathcal{P}(\mathbb{R}^n)$  is sequentially composable if  $F_1(T_1) \subset F_2(0)$ .*

In other words, two funnels are sequentially composable if the “outlet” of one is contained within the “inlet” of the other. A pictorial depiction of this is provided in Figure 2. We note that the sequential composition of two such funnels is itself a funnel.

### 5.2 Exploiting invariances in the dynamics

For our purposes here, it is useful to introduce a slightly generalized notion of sequential composability that will allow us to exploit *invariances* in the dynamics. In particular, the dynamics of large

classes of mechanical systems such as mobile robots are often invariant under certain transformations of the state space. For Lagrangian systems, the notion of “cyclic coordinates” captures such invariances. A cyclic coordinate is a (generalized) coordinate of the system that the Lagrangian does *not* depend on. We can then write the dynamics of the system  $\dot{x} = f(x(t), u(t))$  as a function of a state vector  $x = [x_c, x_{nc}]$  which is partitioned into cyclic coordinates  $x_c$  and non-cyclic coordinates  $x_{nc}$  in such a way that the dynamics only depend on the non-cyclic coordinates:

$$\dot{x} = f(x_{nc}(t), u(t)). \quad (49)$$

For example, the dynamics of a quadrotor or fixed-wing airplane (expressed in an appropriate coordinate system) do not depend on the  $x - y - z$  position of the system or the yaw angle.

Invariance of the dynamics of the system also implies that if a curve  $t \mapsto (x(t), u(t))$  is a valid solution to the dynamics  $\dot{x} = f(x(t), u(t))$ , then so is the transformed solution:

$$t \mapsto (\Psi_c(x(t)), u(t)), \quad (50)$$

where  $\Psi_c$  is a transformation of the state vector along the cyclic coordinates. This allows us to make the following important observation.

**Remark 2.** *Suppose we are given a system whose dynamics are invariant to transformations  $\Psi_c$  along cyclic coordinates  $x_c$ . Let  $F : [0, T] \rightarrow \mathcal{P}(\mathbb{R}^n)$  given by  $t \mapsto F(t)$  be a funnel associated with this system. Then the transformed funnel given by  $t \mapsto \Psi_c(F(t))$  is also a valid funnel. Hence, one can in fact think of invariances in the dynamics giving rise to an infinite family of funnels parameterized by shifts  $\Psi_c(F)$  of a funnel  $F$  along cyclic coordinates of the system.*

Note that here we have implicitly assumed that the feedback controller:

$$u_f(t, x) = u_0(t) + \bar{u}_f(t, \bar{x}) = u_0(t) + \bar{u}_f(t, x - x_0(t)) \quad (51)$$

associated with the funnel has also been transformed to:

$$u_0(t) + \bar{u}_f(t, x - \Psi_c(x_0(t))). \quad (52)$$

In other words, we have transformed the reference trajectory we are tracking by  $\Psi_c$ . Henceforth, when we refer to transformations of funnels along cyclic coordinates we will implicitly assume that the feedback controller has also been appropriately modified in this manner.

These observations allow us to define a generalized notion of sequential composition that exploits invariances in the dynamics. We will refer to this notion as sequential composition *modulo invariances* (MI).

**Definition 3.** *An ordered pair  $(F_1, F_2)$  of funnels  $F_1 : [0, T_1] \rightarrow \mathcal{P}(\mathbb{R}^n)$  and  $F_2 : [0, T_2] \rightarrow \mathcal{P}(\mathbb{R}^n)$  is sequentially composable modulo invariances (MI) if there exists a transformation  $\Psi_c$  of the state along cyclic coordinates such that  $F_1(T_1) \subset \Psi_c(F_2(0))$ .*

Informally, two funnels  $F_1$  and  $F_2$  are sequentially composable in this generalized sense if one can shift  $F_2$  along the cyclic coordinates of the system and ensure that its inlet contains the outlet of  $F_1$ . Figure 3 provides a pictorial depiction of this.

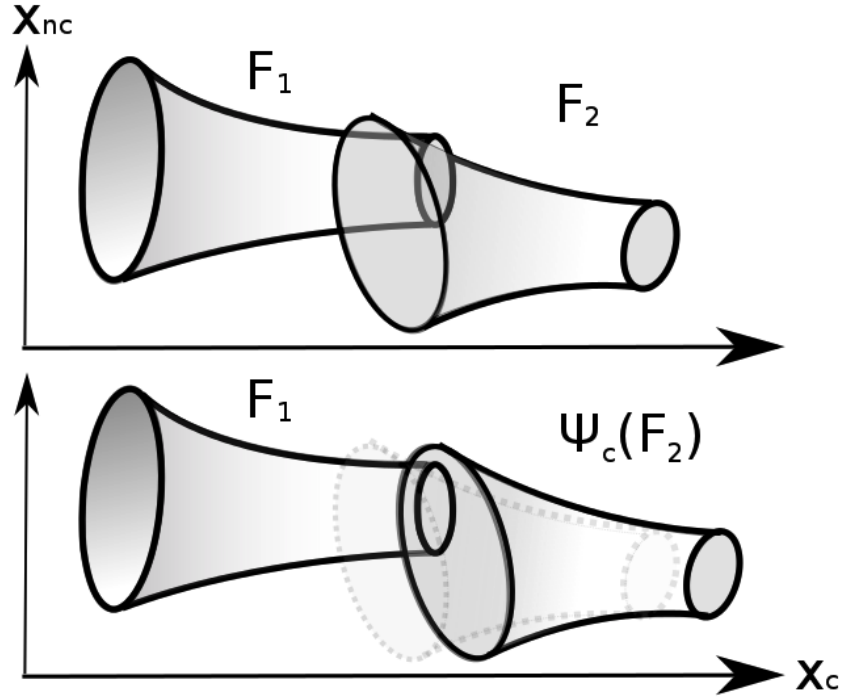


Figure 3: Sequential composition modulo invariances. The top row of the figure shows two funnels that are *not* sequentially composable in the sense of Definition 2. However, as shown in the bottom row of the figure, they *are* sequentially composable in the more general sense of Definition 3. By shifting the funnel  $F_2$  (whose outline is plotted using dotted lines for reference) in the cyclic coordinate ( $x_c$ ), we can ensure that the outlet of  $F_1$  lies in the inlet of this shifted funnel  $\Psi_c(F_2)$ .

One may think of sequential composability MI of funnels as being analogous to the compatibility condition required for sequencing trajectories in the library of a Maneuver Automaton [Frazzoli et al., 2005]. Let  $\pi_{nc}$  denote the projection operator that maps a state  $x = [x_c, x_{nc}]$  to the non-cyclic coordinates  $x_{nc}$ . In order to be able to sequence together two trajectories  $x_1 : [0, T_1] \rightarrow \mathbb{R}^n$  and  $x_2 : [0, T_2] \rightarrow \mathbb{R}^n$ , one requires:

$$\pi_{nc}(x_1(T_1)) = \pi_{nc}(x_2(0)). \quad (53)$$

Note, however that imposing this compatibility condition on the nominal trajectories associated with two funnels is neither necessary nor sufficient for the funnels being sequentially composable MI.

### 5.3 Runtime composability

The two notions of sequential composability we have considered so far allow us to produce new funnels from a given set of funnels by stitching them together appropriately in an offline preprocessing stage. We now introduce another notion of composability that is particularly important for reasoning about how funnels can be executed sequentially at runtime. We will refer to this notion as *runtime composability*.

**Definition 4.** An ordered pair  $(F_1, F_2)$  of funnels  $F_1 : [0, T_1] \rightarrow \mathcal{P}(\mathbb{R}^n)$  and  $F_2 : [0, T_2] \rightarrow \mathcal{P}(\mathbb{R}^n)$  is runtime composable if for all  $x_{out} \in F_1(T_1)$ , there exists a transformation  $\Psi_c$  of the state along cyclic coordinates such that  $x_{out} \in \Psi_c(F_2(0))$ .

In other words, for any state  $x_{out}$  in the outlet of  $F_1$ , one can shift  $F_2$  along cyclic coordinates and ensure that its inlet contains  $x_{out}$ . Hence, we can guarantee that it will be possible to execute the funnel  $F_2$  (after appropriate shifting in the cyclic coordinates) once the funnel  $F_1$  has been executed (though the *particular* shift  $\Psi_c$  required depends on  $x_{out}$  and thus will not be known until runtime). Hence, runtime composability of funnels allows us to exploit invariances in the dynamics of the system at runtime and effectively reuse our robust motion plans in different scenarios. As a simple example, a UAV flying through a cluttered environment can reuse a funnel computed for a certain starting position by shifting the funnel so its inlet contains the UAV's current state.

**Remark 3.** It is easy to see from Definition 4 that two funnels  $F_1$  and  $F_2$  are runtime composable if and only if:

$$\forall x_{out} = [x_c, x_{nc}] \in F_1(T_1), \exists x_{0,c} \text{ s.t. } [x_{0,c}, x_{nc}] \in F_2(0). \quad (54)$$

This condition is simply stating that we can shift the point  $x_{out}$  along cyclic coordinates in such a way that it is contained in the inlet of  $F_2$ . This condition in turn is equivalent to:

$$\pi_{nc}(F_1(T_1)) \subset \pi_{nc}(F_2(0)), \quad (55)$$

where as before  $\pi_{nc}$  denotes the projection onto the non-cyclic coordinates of the state space.

Figure 4 shows two funnels that are *not* sequentially composable MI. However, since  $\pi_{nc}(F_1(T_1)) \subset \pi_{nc}(F_2(0))$ , they *are* runtime composable.

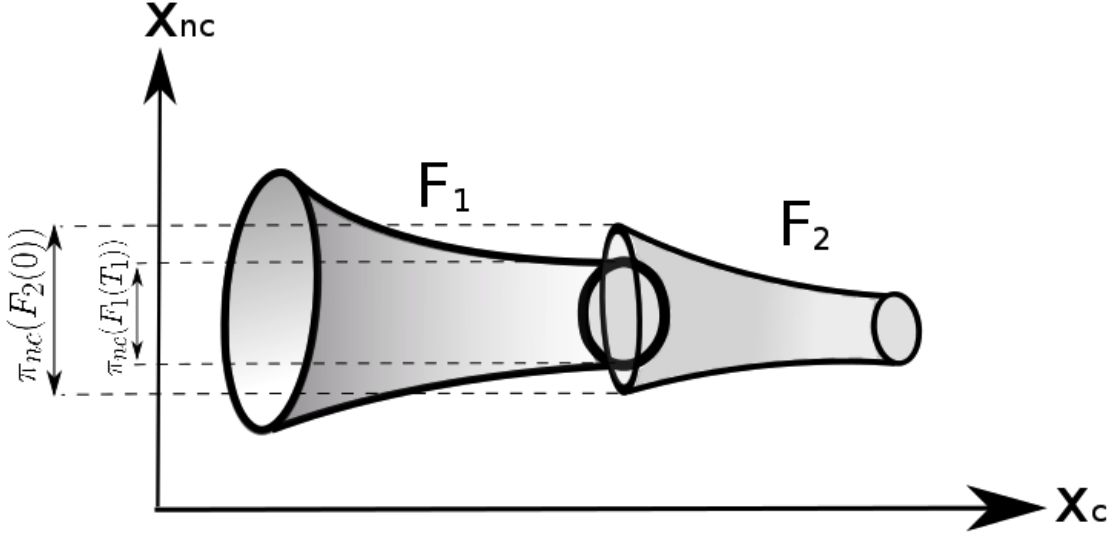


Figure 4: The figure shows two funnels that are *not* sequentially composable MI. However, since  $\pi_{nc}(F_1(T_1)) \subset \pi_{nc}(F_2(0))$ , they *are* runtime composable.

We end our discussion on composability of funnels by noting the following relationship between the three notions of sequential composability we have discussed.

**Remark 4.** *The three notions of sequential composability we have discussed are related as follows:*

$$\text{Sequential composability} \implies \text{Sequential composability MI} \implies \text{Runtime composability}.$$

The first implication is immediate from Definitions 2 and 3. The second implication follows from the following reasoning:

$$\begin{aligned} F_1(T_1) &\subset \Psi_c(F_2(0)) && \text{(Sequential composability MI, ref. Definition 3)} \\ \implies \pi_{nc}(F_1(T_1)) &\subset \pi_{nc}(\Psi_c(F_2(0))) = \pi_{nc}(F_2(0)) && \text{(Runtime composability, ref. Remark 3).} \end{aligned}$$

## 5.4 Checking composability

Given two funnels  $F_1 : [0, T_1] \rightarrow \mathcal{P}(\mathbb{R}^n)$  and  $F_2 : [0, T_2] \rightarrow \mathcal{P}(\mathbb{R}^n)$  defined as  $F_1(t) = \{\bar{x} \in \mathbb{R}^n \mid V_1(t, \bar{x}) \leq \rho_1(t)\}$  and  $F_2(t) = \{\bar{x} \in \mathbb{R}^n \mid V_2(t, \bar{x}) \leq \rho_2(t)\}$  for polynomials  $V_1$  and  $V_2$ , this section describes how we can check sequential composability, sequential composability MI and runtime composability in an offline preprocessing stage.

### 5.4.1 Sequential composability

Sequential composability of  $(F_1, F_2)$  is equivalent to the following condition:

$$V_1(T_1, \bar{x}) \leq \rho_1(T_1) \implies V_2(0, \bar{x}) \leq \rho_2(0). \quad (56)$$



We can thus apply the generalized S-procedure (described in Section 3.2) and check sequential composability using the following simple SOS program:

$$\begin{aligned} \text{Find} \quad & L(\bar{x}) \\ \text{s.t.} \quad & \rho_2(0) - V_2(0, \bar{x}) - L(\bar{x})(\rho_1(T_1) - V_1(T_1, \bar{x})) \text{ is SOS,} \\ & L(\bar{x}) \text{ is SOS.} \end{aligned} \tag{57}$$

#### 5.4.2 Sequential composition MI

In order to check sequential composability MI, we need to search for a shift  $\Psi_c$  along cyclic coordinates of the state such that  $F_1(T_1) \subset \Psi_c(F_2(0))$ . For the important special case in which the sets  $F_1(T_1)$  and  $F_2(0)$  are ellipsoids (corresponding to  $V_1(T_1, \bar{x})$  and  $V_2(0, \bar{x})$  being quadratic<sup>2</sup> in  $\bar{x}$ ), we can cast this search as a semidefinite program (SDP). Suppose the sets  $F_1(T_1)$  and  $F_2(0)$  are given by:

$$F_1(T_1) = \{x \in \mathbb{R}^n \mid (x - x_1(T_1))^T S_1 (x - x_1(T_1)) \leq 1\} \tag{58}$$

$$F_2(0) = \{x \in \mathbb{R}^n \mid (x - x_2(0))^T S_2 (x - x_2(0)) \leq 1\}, \tag{59}$$

where  $x_1 : [0, T_1] \rightarrow \mathbb{R}^n$  and  $x_2 : [0, T_2] \rightarrow \mathbb{R}^n$  are the nominal trajectories around which the funnels were computed and  $S_1$  and  $S_2$  are positive definite matrices. We would like to search for a shift  $\Delta_c \in \mathbb{R}^n$  (where the components of  $\Delta_c$  corresponding to the non-cyclic coordinates are set to zero) such that the ellipsoid:

$$\Psi_c(F_2(0)) = \{x \in \mathbb{R}^n \mid [x - (x_2(0) + \Delta_c)]^T S_2 [x - (x_2(0) + \Delta_c)] \leq 1\} \tag{60}$$

is contained within the ellipsoid  $F_1(T_1)$ . The first step in obtaining the desired SDP is to note that the set  $\Psi_c(F_2(0))$  can be represented equivalently as the image of the unit ball under an affine map:

$$\Psi_c(F_2(0)) = \{Bu + x_2(0) + \Delta_c \mid \|u\|_2 \leq 1\}, \tag{61}$$

where  $B = \text{chol}(S_2)^{-1}$ . Here,  $\text{chol}(S_2)$  is the Cholesky factorization of  $S_2$  (guaranteed to exist and be invertible since  $S_2$  is positive definite). Such a representation is a standard trick in semidefinite programming (see for example [Boyd and Vandenberghe, 2004, Chapter 8.4.2]).

Introducing the notation  $b := -S_1 x_1(T_1)$  and  $c := x_1(T_1)^T S_1 x_1(T_1) - 1$ , the condition that the ellipsoid  $F_1(T_1)$  is a subset of the ellipsoid  $\Psi_c(F_2(0))$  is then *equivalent* to being able to find a scalar  $\lambda > 0$  such that the following matrix semidefiniteness constraint holds ([Boyd and Vandenberghe, 2004, Chapter 8.4.2]):

$$\begin{bmatrix} -\lambda - c + b^T S_1^{-1} b & 0_{1 \times n} & (x_2(0) + \Delta_c + S_1^{-1} b)^T \\ 0_{n \times 1} & \lambda I_{n \times n} & B \\ x_2(0) + \Delta_c + S_1^{-1} b & B & S_1^{-1} \end{bmatrix} \succeq 0. \tag{62}$$

Here, the matrices  $I$  and  $0$  represent the identity matrix and the all-zeros matrix respectively. Since this semidefiniteness condition is linear in  $\lambda$  and  $\Delta_c$ , the problem of searching for these decision variables subject to  $\lambda > 0$  and (62) is a SDP. This SDP will be feasible if and only if  $F_1$  and  $F_2$  are sequentially composable MI.

---

<sup>2</sup>Note that the restriction to quadratic  $V_1(T_1, \bar{x})$  and  $V_2(0, \bar{x})$  is a relatively mild one. We are not imposing any conditions on the degree of  $V_1$  and  $V_2$  at times other than the endpoints.

The problem of checking sequential composability MI in the more general non-ellipsoidal case is not directly amenable to such a SDP based formulation. However, since the problem of checking sequential composability MI reduces to the problem of checking sequential composability for a *fixed*  $\Psi_c$ , we can use the SOS program (57) to verify if a given  $\Psi_c$  yields the desired containment constraint  $F_1(T_1) \subset \Psi_c(F_2(0))$ . One natural choice is to set  $\Psi_c$  such that  $\pi_c(\Psi_c(x_2(0))) = \pi_c(x_1(T_1))$ , where  $\pi_c$  is the projection of the state onto the cyclic coordinates. Intuitively, this corresponds to shifting the funnel  $F_2$  so that the start of its nominal trajectory is lined up along cyclic coordinates with the end of the nominal trajectory of  $F_1$ . If the SOS program is infeasible, a local search around this  $\Psi_c$  could yield the desired shift.

### 5.4.3 Runtime composability

In order to check runtime composability of  $F_1$  and  $F_2$ , we need to check the inclusion  $\pi_{nc}(F_1(T_1)) \subset \pi_{nc}(F_2(0))$ . For the important special case where the sets  $F_1(T_1)$  and  $F_2(0)$  are ellipsoids, we can compute the projections exactly. This is because the projection of an ellipsoid onto a linear subspace is also an ellipsoid (see equation (45) for the exact formula for the projected ellipsoid). Checking if a given ellipsoid contains another is a straightforward application of semidefinite programming [Boyd and Vandenberghe, 2004, Example B.1, Appendix B].

For the more general case, one might hope for a SOS programming based condition for checking  $\pi_{nc}(F_1(T_1)) \subset \pi_{nc}(F_2(0))$ . However, the existential quantifier inherent in the projection (see the equivalent condition (54)) makes it challenging to formulate such SOS conditions. Nevertheless, there exist general purpose tools such as *quantifier elimination* [Collins and Hong, 1998] for checking quantified polynomial formulas such as (54). While the worst-case complexity of doing general purpose quantifier elimination is poor, software packages such as QEPCAD [Brown, 2003] (or dReal [Gao et al., 2013], which is based on a different theoretical framework) can often work well in practice for specialized problems.

## 5.5 Funnel library

A simple but useful generalization of the notions of composability introduced above can be obtained by checking the associated containment conditions at a given time  $\tau_1$  rather than at time  $T_1$ . For example, we will say that the ordered pair of funnels  $(F_1, F_2)$  is sequentially composable at time  $\tau_1$  if  $F_1(\tau_1) \subset F_2(0)$ . We will use similar terminology for the other notions of composability. Given a collection  $\mathcal{F}$  of funnels associated with a dynamical system, we will associate a directed graph  $\mathcal{G}(\mathcal{F})$  whose vertices correspond to funnels  $F \in \mathcal{F}$ . Two vertices corresponding to funnels  $F_i$  and  $F_j$  are connected by a directed edge  $(F_i, F_j)$  if and only if the ordered pair  $(F_i, F_j)$  is runtime composable at some specified time  $\tau_i$ . We will sometimes refer to  $\tau_i$  as the execution time of funnel  $F_i$ .

**Definition 5.** A funnel library FL associated with a given dynamical system is a tuple  $FL = (\mathcal{F}, \mathcal{G}(\mathcal{F}), \mathcal{C}, \{\tau_i\})$ , where  $\mathcal{F}$  is a set of funnels for the dynamical system,  $\mathcal{G}(\mathcal{F})$  is the directed graph representing which funnels are runtime composable,  $\mathcal{C}$  is the set of feedback controllers associated with the funnels in  $\mathcal{F}$ , and  $\{\tau_i\}$  is the set of execution times.

Note that while we do not impose restrictions such as connectedness or strong connectedness on the graph  $\mathcal{G}(\mathcal{F})$ , it may be useful to impose such conditions based on the task at hand. For example, for tasks which require continuous operation (such as a UAV navigating indefinitely through a forest

or a factory arm continuously placing objects onto a conveyor belt), we should require that  $\mathcal{G}(\mathcal{F})$  be strongly connected (since if  $\mathcal{G}(\mathcal{F})$  is not strongly connected, we are ruling out the possibility of executing certain funnels in the future). On a similar note, properties of the graph such as its *diameter* or *girth* may be related to the efficiency with which a certain task can be accomplished. Identifying which graph theoretic properties should be imposed on  $\mathcal{G}(\mathcal{F})$  for different tasks is an interesting research avenue, but we do not pursue this in the present work.

## 6 Online Planning

Given a funnel library  $\text{FL} = (\mathcal{F}, \mathcal{G}(\mathcal{F}), \mathcal{C}, \{\tau_i\})$  computed offline, we can proceed to use it for robust real-time planning in previously unseen environments. The robot’s task specification may be in terms of a goal region that must be reached (as in the case of a manipulator arm grasping an object), or in terms of a nominal direction the robot should move in while avoiding obstacles (as in the case of a UAV flying through a forest or a legged robot walking over rough terrain). For the sake of concreteness, we adopt the latter task specification although one can adapt the contents of this section to the former specification. We further assume that the robot is provided with regions in the configuration space that obstacles are guaranteed to lie in and that the robot’s sensors only provide this information up to a finite (but receding) spatial horizon. Our task is to choose funnels from our library in a way that avoids obstacles while moving forwards in the nominal direction.

The key step in our real-time planning approach is the selection of a funnel from the funnel library that doesn’t intersect any obstacles in the environment. This selection process is sketched in the ReplanFunnel algorithm (Algorithm 3). Given the current state  $x$  of the robot and the locations and geometry of obstacles  $\mathcal{O}$  in the environment, the algorithm searches through the funnels in the library that are runtime composable with the previous funnel that was executed. We assume that the funnels are ordered in a preference list. As an example, this ordering can be based on likely progress towards the goal or by aggressiveness of the maneuvers (less aggressive maneuvers are given preference) for a UAV. For each funnel  $F_i$ , the algorithm tries to find a shift  $\Psi_c$  along cyclic coordinates of the system such that the shifted funnel  $\Psi_c(F_i)$  satisfies two properties: (i) the current state  $x$  is contained in the inlet of the shifted funnel, (ii) the projection of the shifted funnel onto the coordinates of the state space corresponding to the configuration space doesn’t intersect any obstacles in  $\mathcal{O}$ . If we are able to find such a shift, we are *guaranteed* that the system will remain collision-free when the funnel is executed despite the uncertainties and disturbances that the system is subjected to.

The simplest way to try to choose  $\Psi_c$  is to set it such that the nominal trajectory  $x_i$  associated with the funnel lines up with the current state in the cyclic coordinates (i.e., using the notation of Section 5,  $\pi_c(\Psi_c(x_i(0))) = \pi_c(x)$ ). Intuitively, this corresponds to shifting the funnel so that it is executed from the current location of the robot. We can then use standard collision-checking libraries such as the Bullet Collision Detection & Physics Library [Coumans et al., 2014] to check if  $\Psi_c(F_i)$  (projected onto the configuration space) intersects any obstacles. We will discuss more sophisticated ways of finding  $\Psi_c$  in Section 6.1.

If the search for a collision-free funnel in Algorithm 3 doesn’t succeed, we assume that there is a fail-safe maneuver that can be executed to keep the robot safe. For a ground vehicle, this could be coming to a stop while for a quadrotor or fixed-wing airplane this may involve transitioning to a hover or propeller-hang mode.

Algorithm 4 provides a sketch of the real-time planning and control loop, which applies the

---

**Algorithm 3** ReplanFunnel

---

```
1: Inputs:  $x$  (current state of system),  $\mathcal{O}$  (reported obstacles in environment), previousFunnel  
   (previous funnel that was executed)  
2: for  $i = 1, \dots, \#(\mathcal{F})$  such that  $(\text{previousFunnel}, F_i) \in \mathcal{G}(\mathcal{F})$  do  
3:   success  $\Leftarrow$  Find a shift  $\Psi_c$  along cyclic coordinates such that  $x$  is contained in the inlet of  
    $\Psi_c(F_i)$  and  $\Psi_c(F_i)$  is collision-free w.r.t.  $\mathcal{O}$   
4:   if success then  
5:     return  $\Psi_c(F_i)$   
6:   end if  
7: end for  
8: return  $F_{\text{failsafe}}$ 
```

---

replanFunnel algorithm in a receding-horizon manner. At every control cycle, the robot's sensors provide it with a state estimate and report the locations and geometry of the set of obstacles  $\mathcal{O}$  in the sensor horizon. The algorithm triggers a replanning of funnels if any of the following three criteria are met: (i) if the system has executed the current funnel  $F_i$  for the associated execution time  $\tau_i$ , (ii) if the current state of the system is no longer in the funnel being executed, or (iii) if the current funnel being executed is no longer collision-free. In principle, (ii) should not happen. However, in practice this can happen if the system received a disturbance that was larger than the ones taken into account for the funnel computations. Option (iii) can happen if the robot's sensors report new obstacles that were previously unseen.

---

**Algorithm 4** Real-time planning loop

---

```
1:  $x \Leftarrow$  Initialize current state of the robot  
2:  $\mathcal{O} \Leftarrow$  Initialize obstacles in sensor horizon  
3:  $F_i \in \mathcal{F} \Leftarrow$  Initialize current planned funnel  
4: for  $t = 0, \dots$  do  
5:    $x \Leftarrow$  Update current state of robot  
6:    $\mathcal{O} \Leftarrow$  Update obstacles in sensor horizon  
7:   replan  $\Leftarrow$  Check if we have finished executing current funnel  $F_i$  for the associated execution  
   time  $\tau_i$   
8:   insideFunnel  $\Leftarrow$  Check if current state is still inside the current funnel  $F_i$  being executed  
9:   collisionFree  $\Leftarrow$  Check if current funnel  $F_i$  is still collision-free with  $\mathcal{O}$   
10:  if replan or  $\neg$ insideFunnel or  $\neg$ collisionFree then  
11:     $F_i \Leftarrow$  ReplanFunnels( $x, \mathcal{O}, F_i$ )  
12:  else  
13:    apply feedback control input  $u$  associated with current funnel  $F_i$   
14:  end if  
15: end for
```

---

Of course, several variations on our real-time planning approach are possible. In ReplanFunnel, instead of choosing the first collision-free funnel found in the preference list, we can choose the funnel that has maximal clearance from the obstacles. In general, the funnel primitives provide a discrete action space which can be searched by any heuristic planner - the primary considerations

here are the additional constraint of containment of the current state in the inlet and the moderately more significant cost of collision checking.

## 6.1 Shifting funnels at runtime

The main step in Algorithm 3 is the search for a shift  $\Psi_c$  along cyclic coordinates such that the shifted funnel  $\Psi_c(F_i)$  will be collision-free with respect to the obstacles in  $\mathcal{O}$  while containing the current state  $x$  in its inlet:

$$\text{Find} \quad \Psi_c \tag{63}$$

$$\text{s.t.} \quad x \in \Psi_c(F_i(0)), \tag{64}$$

$$\pi_{conf}(\Psi_c(F_i)) \cap \mathcal{O} = \emptyset.$$

Here,  $\pi_{conf}$  is the projection onto the configuration space variables of the state space. This optimization problem is non-convex in general since the free-space of the environment is non-convex. However, the number of decision variables is very small. In particular, if we parameterize the shift  $\Psi_c$  by a vector  $\Delta_c \in \mathbb{R}^n$  (where the coordinates of  $\Delta_c$  corresponding to the non-cyclic coordinates are set to zero) such that  $\Psi_c(x) = x + \Delta_c$ , the number of decision variables is equal to the number of cyclic coordinates of the system.

We can thus apply general-purpose nonlinear optimization tools such as gradient-based methods to solve this problem. In particular, the first constraint is equivalent to checking that the value of the Lyapunov function  $V(0, \bar{x}) = V(0, x - (x_i(0) + \Delta_c))$  at time 0 is less than or equal to  $\rho(0)$  (recall that the funnel is described as the  $\rho(t)$  sub-level set of the function  $V(t, \bar{x})$ ). As in Section 4,  $x_i$  here is the nominal trajectory corresponding to the funnel  $F_i$ . The second constraint can be evaluated using off-the-shelf collision-checking libraries.

Despite the small number of decision variables, for some applications general-purpose nonlinear optimization may be too slow to run in real-time. For the important special case where the cyclic coordinates form a subset of the configuration space variables (e.g., for a UAV), we propose another approach that allows us to search over a restricted family of shifts  $\Psi_c$  but has the advantage of being posed using *convex* quadratic constraints. The first observation is that the containment constraint (64) is a convex quadratic constraint for the case where the inlet of the funnel is an ellipsoid (i.e., the function  $V(0, \bar{x})$  is a positive definite quadratic). If this condition doesn't hold, we can find an ellipsoidal inner approximation of the inlet of the funnel (e.g., by solving a simple SOS program).

Next, we seek to find a set of convex constraints that will guarantee non-collision of the funnel. We will assume that  $\pi_{conf}(F_i)$  is represented as a union of convex segments  $\mathcal{S}_k$ . For each such segment, we can find collision normals  $n_{jk}$  and collision distances  $d_{jk}$  to each obstacle  $o_j \in \mathcal{O}$  (these are easily extracted from a collision-checking software). Figure 5 provides an illustration of this for a single convex segment  $\mathcal{S}_1$ . The two regions colored in red are obstacles. The collision normals are  $n_{11}$  and  $n_{21}$ . By definition, collision normals provide us with constraints such that any shift  $\Delta_c$  of the segment  $\mathcal{S}_1$  satisfying the linear constraint  $n_{jk}^T \Delta_c < d_{jk}$  will be collision-free. The region corresponding to this is shaded in green in the figure.

The constraints described above (containment of the current state in an ellipsoid and the linear constraints given by the collision normals) form a special case of convex Quadratically Constrained Quadratic Programs (QCQPs), for which there exist very mature software packages. For our examples in Section 7, we use the FORCES Pro package [Domahidi and Jerez, 2014]. This generates

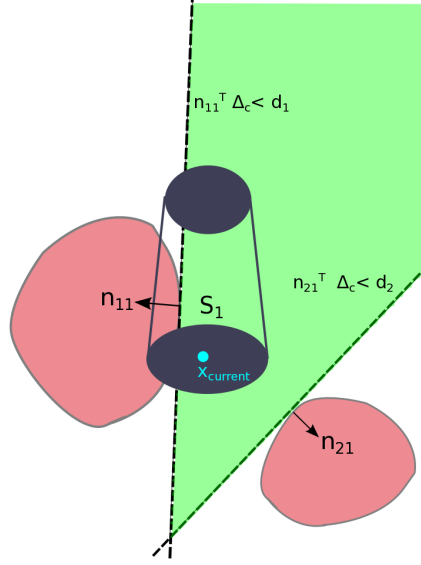


Figure 5: The two red regions are obstacles. The green region represents the set of allowable shifts of the funnel segment that satisfy the linear constraints given by the collision normals and collision distances.

solver code tailored to the specific optimization problem at hand and was faster in our experience than using general-purpose QCQP solvers.

## 7 Examples

### 7.1 Ground Vehicle Model

As our first example we consider a ground vehicle model based on the Dubins car [Dubins, 1957] navigating an environment of polygonal obstacles. A pictorial depiction of the model is provided in Figure 6. The vehicle is constrained to move at a fixed forward speed and can control the second derivative of its yaw angle  $\psi$ . We introduce uncertainty into the model by assuming that the speed of the vehicle is only known to be within a bounded range and is potentially time-varying. The full non-linear dynamics of the system are then given by:

$$\mathbf{x} = \begin{bmatrix} x \\ y \\ \psi \\ \dot{\psi} \end{bmatrix}, \quad \dot{\mathbf{x}} = \begin{bmatrix} -v(t) \sin \psi \\ v(t) \cos \psi \\ \dot{\psi} \\ u \end{bmatrix} \quad (65)$$

with the speed of the plane  $v(t) \in [9.0, 11.0]$  m/s. The control input is bounded in the range  $[-1000, 1000]$  rad/s<sup>2</sup>.

The trajectory library,  $\mathcal{T}$ , computed for the ground vehicle consists of 20 trajectories and is shown in Figure 7(a). The trajectories  $x_i(t) : [0, T_i] \mapsto \mathbb{R}^4$  and the corresponding nominal open-loop control inputs were obtained via the direct collocation trajectory optimization method [Betts, 2001] for the vehicle dynamics in (65) with  $v(t) = 10$  m/s. The initial state  $x_i(0)$  was constrained to be

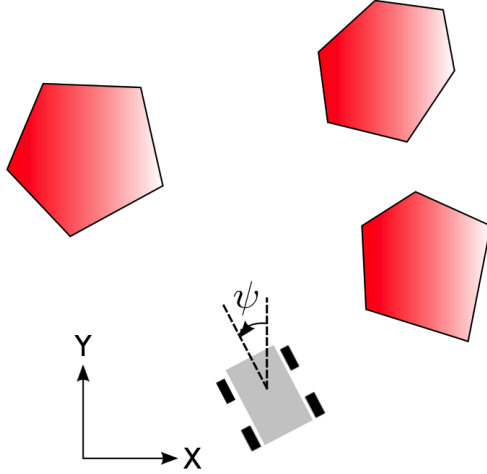


Figure 6: Illustration of the ground vehicle model.

$[0, 0, 0, 0]$  and the final state  $x_i(T_i)$  was varied in the  $x$  direction while keeping the  $y$  component fixed. We locally minimized a cost of the form:

$$J = \int_0^{T_i} [1 + u_0(t)^T R(t) u_0(t)] dt$$

where  $R$  is a positive-definite matrix. We constrained the nominal control input to be in the range  $[-500, 500]$  rad/s<sup>2</sup> to ensure that feedback controllers computed around the nominal trajectories do not immediately saturate.

For each  $x_i(t)$  in  $\mathcal{T}$  we obtain controllers and funnels using the method described in Section 4. In order to obtain polynomial dynamics, we Taylor expanded the dynamics of the system around the nominal trajectory to degree 3. The approach from Section 4.2.2 was used to synthesize a (time-varying) linear feedback controller around each trajectory while the methods described in Section 4.2.1 and 4.2.3 were used to take into account the parametric uncertainty and input saturations that the system is subject to. As described in Section 4.3.2, we used a time-varying LQR controller to initialize the funnel computations. The computation time for each funnel was approximately 5-10 minutes. A subset of the funnels is shown in Figure 7(b). Note that the four-dimensional funnels have been projected down to the  $x - y$  dimensions for the purpose of visualization.

The resulting funnel library was employed by Algorithm 4 for planning in real-time through environments with randomly placed obstacles. Figure 8 shows the funnels that were executed in order to traverse a representative environment. The obstacle positions were randomly generated from a spatial Poisson process (with a density/rate parameter of 0.6). Two further “barrier” obstacles were placed on the sides of the environment to prevent the vehicle from leaving the region containing obstacles. The planner was provided with a sensor horizon of 3m in the  $y$  direction (forwards) and  $\pm 2$ m in the  $x$  direction (side-to-side) relative to the position of the vehicle. Only obstacles in this sensor window were reported to the planner at every instant in time. The execution times  $\tau_i$  for each funnel were set such that replanning occurred once 80% of the funnel was executed. The parametric uncertainty in the speed of the vehicle was taken into account in our simulation by randomly choosing a speed  $v(t) \in \{9.0, 11.0\}$  m/s after every execution time period has elapsed.

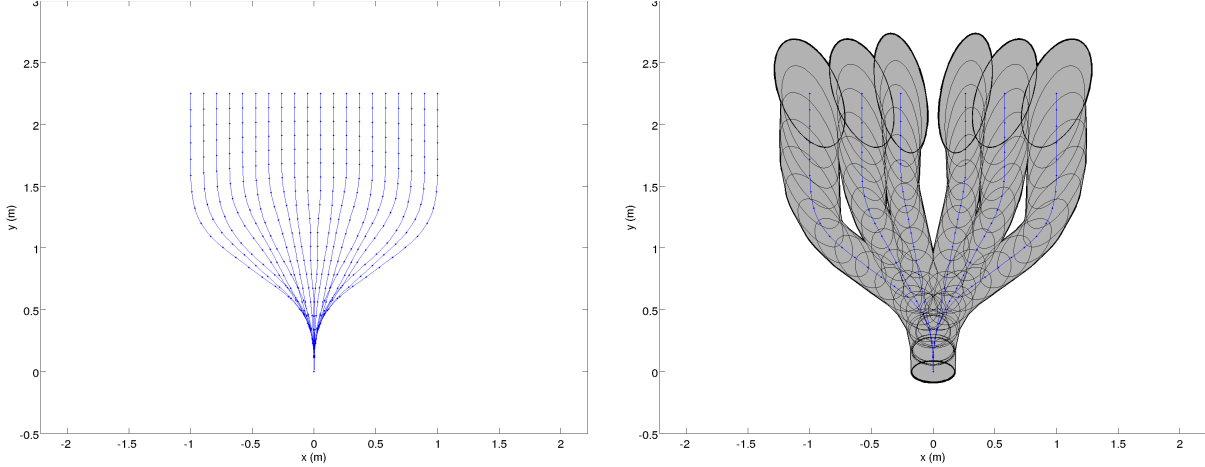


Figure 7: The plot on the left shows the trajectory library for the ground vehicle model. The plot on the right shows a selection of funnels from the funnel library projected onto the  $x - y$  plane.

The real-time planner employs the QCQP-based algorithm from Section 6.1 for shifting funnels in the  $x - y$  directions (we did not exploit invariances in the yaw dimension of the state space in order to ensure that the vehicle moves in the forwards direction and doesn't veer off to the sides). We use the FORCES Pro solver [Domahidi and Jerez, 2014] for our QCQP problems. This resulted in our implementation of the real-time planner running at approximately 40 – 50 Hz.

We performed extensive simulation experiments to compare our funnel library based robust planning approach with a more traditional trajectory library based method. In order to facilitate a meaningful comparison, we used the underlying trajectory library corresponding to our funnel library. The trajectory-based planner employs essentially the same outer-loop as our funnel-based approach (Algorithm 4). The key difference is that the planner chooses which maneuver to execute by evaluating which trajectory has the maximal clearance from the obstacles (as measured by Euclidean distance):

$$\underset{i,j}{\operatorname{argmax}} \operatorname{dist}(x_i, o_j) \quad (66)$$

where  $x_i(t)$  in  $\mathcal{T}$  is a trajectory in the library and  $o_j \in \mathcal{O}$  is an obstacle in the environment. Once a maneuver is chosen based on this metric, a time-varying LQR feedback controller computed along this trajectory is applied (the same LQR controller that is used to initialize the funnel computations).

To compare the two planners, we generated 100 obstacle environments randomly as described previously. For each environment, we ran the different planning algorithms until there was a collision of the vehicle with an obstacle. The distance in the  $y$  direction at the time of collision was recorded for each run. Figure 9 compares the performance of the different approaches. For each distance on the x-axis of the plot the height of the bar indicates the number of runs for which the vehicle traveled beyond this distance. As is evident from the plot, our funnel library based approach provides a significant advantage over the trajectory-based method.



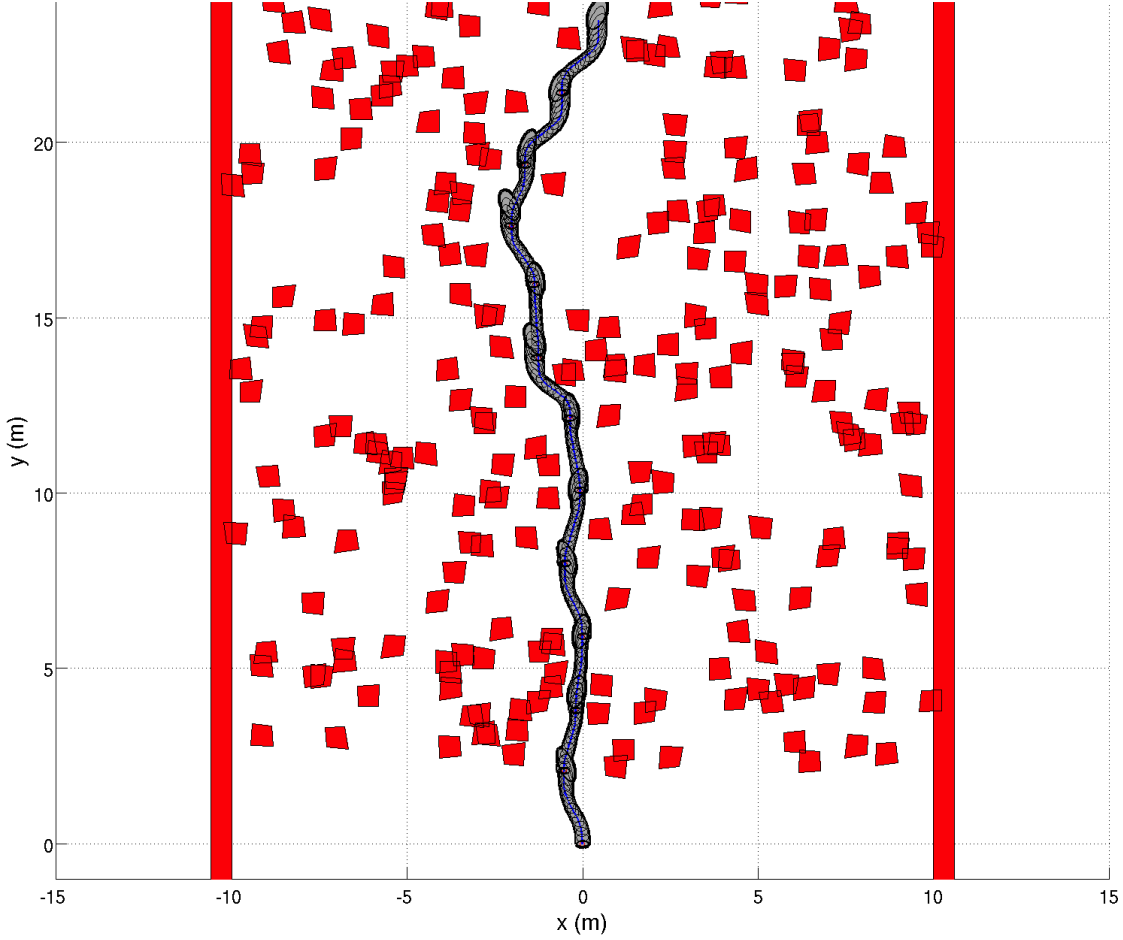


Figure 8: This plot shows the funnels that were executed in order for the ground vehicle model to traverse a randomly generated obstacle environment using the funnel library based real-time planning approach.

## 7.2 Hardware experiments on a fixed-wing airplane

In this section, we will validate the key components of the approach presented in this paper on a small fixed-wing airplane performing a challenging obstacle avoidance task. The goal of these hardware experiments is to answer the following important practical questions:

- Can we obtain models of a real-world challenging nonlinear dynamical system that are accurate enough to compute funnels that are valid in reality?
- Can we implement the real-time planning algorithm described in Section 6 to operate at the required rate given realistic computational constraints?
- Can we demonstrate our planning algorithm on a realistic and challenging obstacle avoidance task?

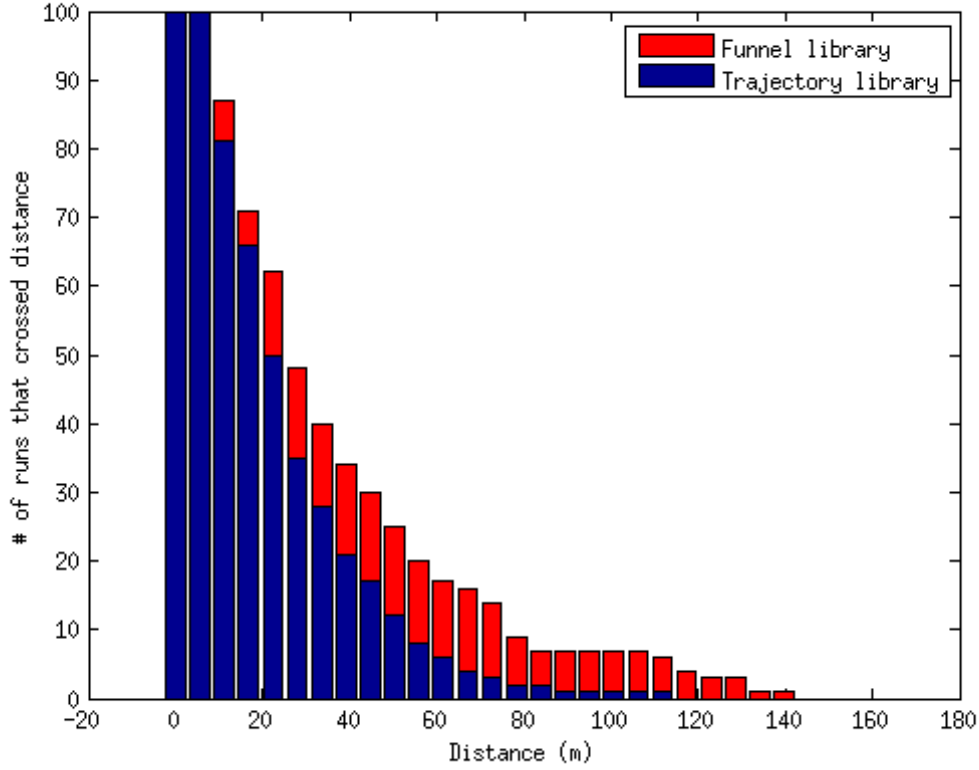


Figure 9: A bar plot comparing the performance of the funnel library approach with one based on a trajectory library.

### 7.2.1 Hardware platform

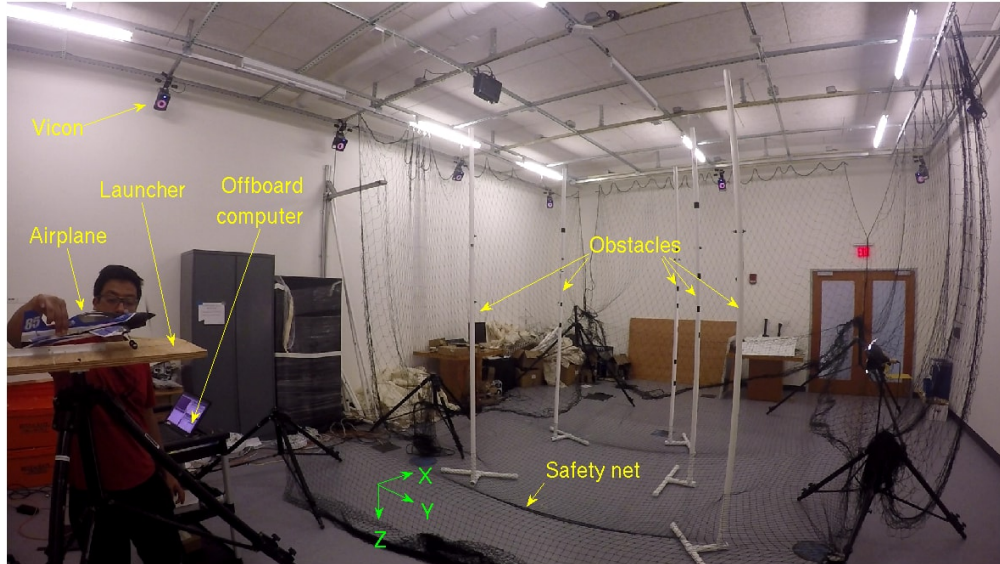
The hardware platform chosen for these experiments is the SBach RC airplane manufactured by E-flite shown in Figure 10(a). The airplane is very light (76.6 g) and highly maneuverable, thus allowing for dramatic obstacle avoidance maneuvers in a tight space. The control inputs to the SBach are raw servo commands to the control surfaces (ailerons, rudder, elevator) and a raw throttle setting. These commands are sent through a modified 2.4 GHz RC transmitter at an update rate of 50 Hz.

### 7.2.2 Task and experimental setup

The experimental setup is shown in Figure 10(b). The airplane is launched from a simple rubber-band powered launch mechanism at approximately 4 – 5 m/s. The goal is to traverse the length of the room while avoiding the obstacles placed in the experimental arena. The airplane’s planner is *not* informed where the obstacles are beforehand; rather, the obstacle positions and geometry are reported to the planner only once the airplane clears the launcher. This simulates the receding horizon nature of realistic obstacle avoidance tasks where the obstacle positions are not known beforehand and planning decisions must be taken in real-time. The experiments are performed in a



(a) The E-flite SBach RC airplane used for hardware experiments.



(b) Experimental setup and coordinate system.

Figure 10: Airplane hardware and experimental setup.

Vicon motion capture arena that reports the airplane and obstacle poses at 120 Hz. All the online computation is performed on an off-board computer with four Intel i7 2.9GHz processors and 16 GB RAM.

### 7.2.3 Modeling and system identification

Our dynamics model of the airplane is based on the model described in [Sobolic, 2009] ([Stevens and Lewis, 1992] is also a good reference for modeling fixed-wing airplanes). The model has 12 states  $[x, y, z, \phi, \theta, \psi, \dot{x}, \dot{y}, \dot{z}, P, Q, R]$ . Here,  $+x$  is in the forward direction,  $+y$  is to the right and  $+z$  is downwards as depicted in Figure 10(b) (this is the standard North-East-Down coordinate frame used in aeronautics). The states  $\phi, \theta, \psi$  are the roll, pitch and yaw angles. The variables  $P, Q, R$  are the components of the angular velocity expressed in the body coordinate frame. The control inputs of the model are the angles of the ailerons, rudder and elevator, along with the speed of the propellor. Thus, we have 4 control inputs since the ailerons are coupled to deflect in opposite directions by the commanded magnitude.

The airplane is treated as a rigid body with aerodynamic and gravitational forces acting on it. Here, we provide a brief description of our model of the aerodynamic forces:

**Propellor thrust** The thrust from the propellor is proportional to the square of the propellor speed. The constant of proportionality was obtained by hanging the airplane (with the propellor pointing downwards) from a digital fish scale and measuring the thrust produced for a number of different throttle settings.

**Lift/drag on aerodynamic surfaces** The lift and drag forces on the ailerons, rudder, elevator and tail of the airplane were computed using the flat plate model. The flat plate model was also used as a baseline for the lift and drag coefficients of the wings, but an angle-of-attack dependent correction term was added. This correction term was fit from experimental data obtained from passive (i.e., unactuated) flights in a manner similar to [Moore, 2014]. Since lift and drag forces are dependent on the airspeed over the aerodynamic surface, we need to take into account the effect of “prop-wash” (i.e. the airflow from the propellor). The relationships between the throttle speed command and the propellor downwash speed over the different control surfaces were measured using a digital anemometer in a manner similar to [Sobolic, 2009].

**Body drag** The drag on the airplane body is approximated as a quadratic drag term whose drag coefficient is fit from data.

As described above, many of the parameters in the model were obtained directly from physical experiments and measurements. However, some model parameters are more difficult to measure directly. These include the moments of inertia of the airplane and the coefficient of drag associated with the airplane body. The prediction error minimization method in the Matlab System Identification Toolbox [Ljung, 2007] was used to fit these parameters and to fine-tune the measured parameters. In particular, we collected data from 15-20 flights (each lasting approximately 0.5–0.7 seconds) where the control inputs were excited using sinusoidal signals of varying frequency and amplitude.

#### 7.2.4 Funnel validation

The first major goal of our hardware experiments was to demonstrate that our model of the SBach airplane is accurate enough to compute funnels that are truly valid in reality. To this end, we computed a funnel (shown in Figure 11(a)) for the airplane using the approach described in Section 4. We first estimated the set of initial states that the launcher mechanism causes the airplane to start off in (here, by “initial state” we mean the state of the airplane as soon as it has cleared the launcher mechanism). This was done by fitting an ellipsoid around the initial states observed from approximately 50 experimental trials. We then used direct collocation trajectory optimization [Betts, 2001] to design an open-loop maneuver that makes the airplane bend towards the left. The initial state of the trajectory is constrained to be equal to the mean of the experimentally observed initial states and the control inputs are constrained to satisfy the limits imposed by the hardware. Next we computed a time-varying LQR controller around this nominal trajectory. This controller was tuned largely in simulation to ensure good tracking of the trajectory from the estimated initial condition set. The resulting closed-loop dynamics were then Taylor expanded around the nominal trajectory to degree 3 in order to obtain polynomial dynamics. Finally, we used SOS programming to compute the funnel depicted in Figure 11(a). The inlet of the funnel was constrained to contain the experimentally estimated set of initial conditions. We observed that the tuned TVLQR controller does not saturate the control inputs for the most part and thus we did not find it necessary to take input saturations into account in our funnel computation. Further, we wanted to assess the validity of our funnel for the nominal dynamics model of the airplane and did not take into account any uncertainty in the model. The funnel computation took approximately 1 hour.

We validate the funnel shown in Figure 11(a) with 30 experimental trials of the airplane executing the maneuver corresponding to the funnel. The airplane is started off in different initial conditions in the inlet of the funnel and the TVLQR controller is applied for the duration of the maneuver. Figure 12 shows still images of a sample flight of the airplane executing the maneuver with the funnel superimposed onto the images. A video with a visualization of the funnel and flights through it is available online<sup>3</sup>.

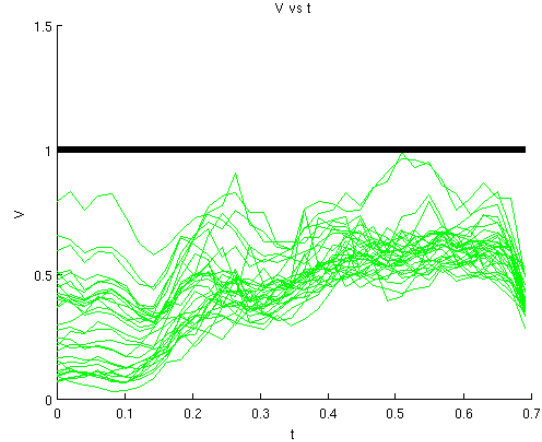
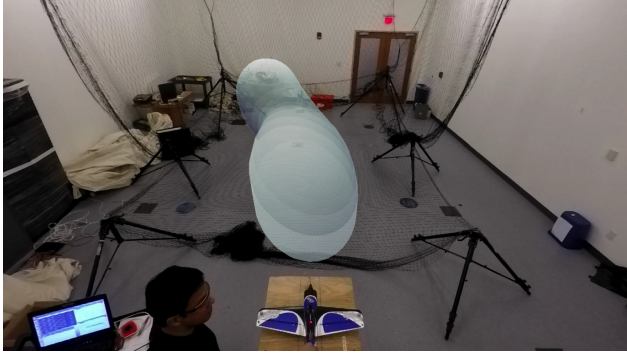
Figure 11(b) provides a more quantitative perspective on the flights. In particular, the figure shows the value of the Lyapunov function  $V(\bar{x}, t)$  as a function of time achieved during the 30 experimental trials. Here, the Lyapunov function has been normalized so that the 1-level set corresponds to the boundary of the funnel. As the plot illustrates, all 30 trajectories remain inside the computed 12 dimensional funnel for the entire duration of the maneuver. This suggests that our model of the airplane is accurate enough to produce funnels that are indeed valid for the hardware system.

#### 7.2.5 Obstacle avoidance experiments

The second major goal of our hardware experiments was to demonstrate the funnel library based real-time planning algorithm proposed in Section 6 on the obstacle avoidance task described in Section 7.2.2. Our first step was to design a rich trajectory library consisting of a large number of different maneuvers. We initialized the library with the maneuver from Section 7.2.4 and augmented it by computing trajectories with varying final states. In particular, the library consists of 40 trajectories which were obtained by discretizing the final state in the  $y$  and  $z$  coordinates and using

---

<sup>3</sup><https://youtu.be/cESFpLgSb50>



- (a) A depiction of the funnel that was validated on hardware. The funnel has been projected down to the  $x - y - z$  coordinates of the state space and then re-projected onto the camera image.
- (b) The value of the Lyapunov function ( $V$ ) plotted as a function of time for 30 different trials of the airplane started from different initial conditions in the inlet of the funnel. The 1-sublevel set of the Lyapunov function corresponds to the funnel (i.e., a Lyapunov function of 1 or less corresponds to the airplane being inside the funnel). All 30 of the trajectories remain inside the computed funnel for the entire duration of the maneuver.

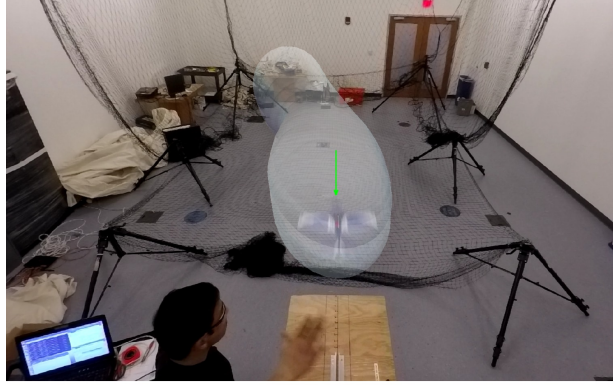
Figure 11: Validating funnels on the SBach fixed-wing airplane.

direct collocation trajectory optimization to compute locally optimal trajectories for the airplane model described in Section 7.2.3. The  $x - y - z$  components of this trajectory library are depicted in Figure 13, with the trajectory from Section 7.2.4 highlighted in blue.

For each trajectory in our library, we computed a TVLQR controller with the same state/action costs as the controller for the maneuver in Section 7.2.4. As in Section 7.2.4, we used SOS programming to compute funnels for each trajectory in the library. We note that since the dynamics of the airplane are symmetric with respect to reflection about the  $x$  axis, we were able to halve the amount of computation involved in constructing the trajectory/funnel library by exploiting this symmetry.

As mentioned in Section 7.2.2, the positions and geometry of the obstacles are not reported to the planner until the airplane has cleared the launcher. This forces planning decisions to be made in real-time. We use the planning algorithm described in Section 6 to choose a funnel from our library. The planner employs the QCQP-based algorithm from Section 6.1 for shifting funnels in the  $x - y - z$  directions. As in the other examples considered in this paper, we use the FORCES Pro solver [Domahidi and Jerez, 2014] for our QCQP problems. If no satisfactory funnel is found by the planner, we revert to a “failsafe” option which involves switching off the propellor and gliding to a halt. A more sophisticated failsafe would be to attempt to transition to a “propellor-hang” mode. However, we found that our failsafe provides adequate protection to the airplane’s hardware as it usually glides on to the safety net before colliding with any obstacles. Finally, we note that since the experimental arena is quite limited in space, we do not replan funnels once one has been chosen; the airplane executes the feedback controller corresponding to the chosen funnel for the

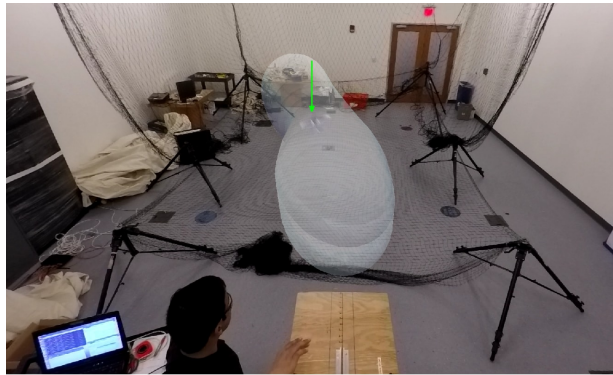




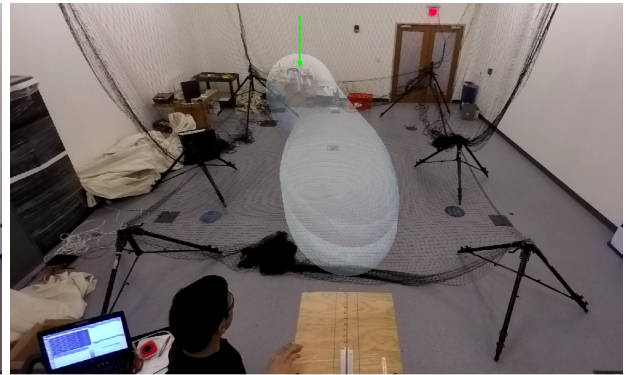
(a)



(b)



(c)



(d)

Figure 12: Still images of the SBach flying through a funnel. The funnel has been projected down to the  $x - y - z$  coordinates of the state space and then reprojected onto the camera image.

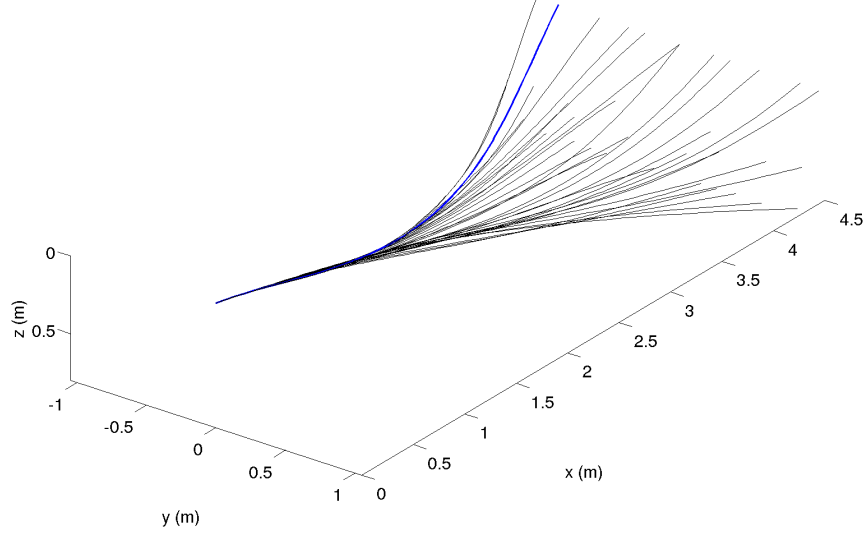


Figure 13: Trajectory library for the SBach airplane. The library consists of 40 different maneuvers. The maneuver from Section 7.2.4 is highlighted in blue.

whole duration of the flight.

We tested our approach on 15 different obstacle environments of varying difficulty. These environments are shown in Figures 14 and 15. The obstacles include poles of different lengths in varying orientations and also a hoop of diameter equal to 0.9 m (as a reference the airplane’s wingspan is 0.44 m, thus only leaving 0.23 m of margin on either side of the airplane assuming it passes through the center of the hoop). We model the poles as cuboids with heights equal to that of the poles and widths equal to the diameter. The hoop is approximated with eight polytopic segments (see Figure 17).

Figure 16 presents a more quantitative perspective on the obstacle environments. Here we have plotted a histogram of the gaps between obstacles in the environment and compared it to the wingspan of the airplane. In particular, for each obstacle in a given environment we consider the distance<sup>4</sup> to the closest obstacle that is at least 5 cm away (the 5 cm threshold is chosen to prevent obstacles that are right next to each other being considered as having a small gap. For example, the obstacle closest to one of the horizontal poles in the first environment in Figure 14 should be the other horizontal pole and not the adjacent vertical pole). As the histogram illustrates, a significant fraction (approximately 35%) of the gaps are less than the airplane wingspan and about 66% of the gaps are less than two wingspans. Of course, it is worth noting that not all of the gaps greater than the wingspan are in fact negotiable (e.g., obstacles placed far apart along the  $x$  direction).

A video of the airplane traversing a few representative environments is available online<sup>5</sup>. Out of the 15 environments the airplane was able to successfully negotiate 14 of them, thus demonstrating the efficacy of our real-time planner on this challenging task. The single failure case occurred on the environment shown at the bottom of Figure 15, where the airplane clips one of the poles close to

<sup>4</sup>Here, the distance between obstacles is defined in the usual way for sets. In particular, for any pair of obstacles  $O_1$  and  $O_2$ , we define the distance between them as  $\min_{x_1 \in O_1, x_2 \in O_2} \|x_1 - x_2\|_2$ .

<sup>5</sup><https://youtu.be/cESFpLgSb50>





Figure 14: Environments 1-8 on which the online planning algorithm was tested. The obstacles include poles of different lengths in varying orientations and also a hoop of diameter equal to 0.9 m.





Figure 15: Environments 9-15 on which we tested our planning algorithm. The bottom most image shows the only failure case. Here the airplane brushed one of the obstacles on its way across the room.

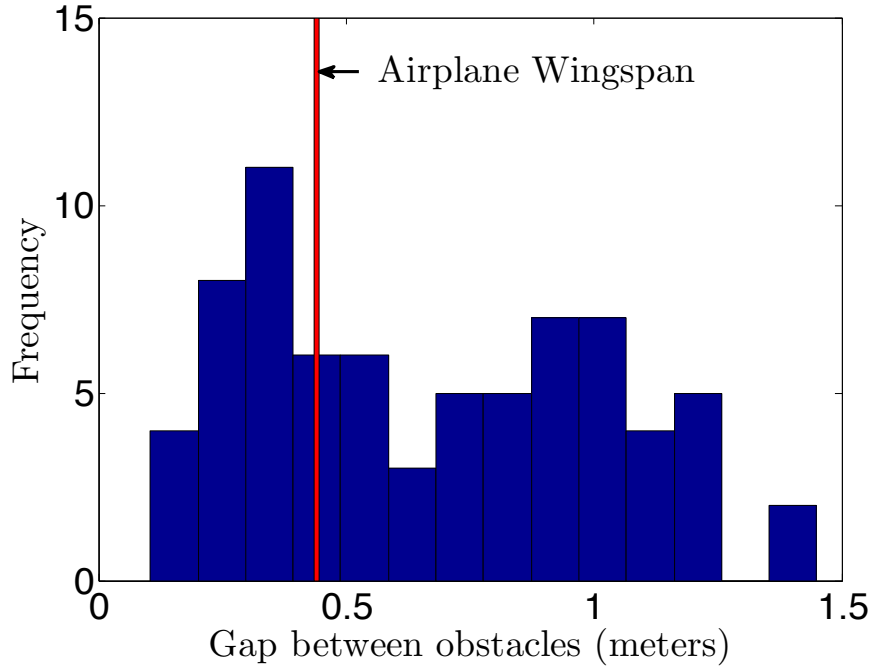


Figure 16: Histogram of gaps between objects in our test environments compared with the airplane’s wingspan (0.44 m). As the plot shows, a significant number of the gaps between obstacles are less than then wingspan.

the end of its flight.

Figure 17 presents the output of our real-time planner on four of the more challenging environments. In particular we plot the funnel chosen by the planner (which have been shifted using the QCQP-based algorithm presented in Section 6.1) alongside an image sequence showing the airplane executing the plan. We note that the increased expressivity afforded to us by the ability to shift funnels in the cyclic coordinates has a large impact on the planner being able to find collision free funnels. Perhaps the best example of this is the environment which contains the hoop (top row of Figure 17). Without the ability to make small adjustments to the funnels, the chances of finding a collision free funnel are extremely low (we would require a funnel that passes almost exactly through the center of the hoop). Figure 18 compares the output of the planner with and without applying the QCQP-based algorithm for shifting funnels. As we can observe, the best funnel found in the former case is well in collision with the obstacles while in the latter case the planner is able to find a collision free funnel. This illustrates the crucial role that exploiting invariances plays in the success of the planner on this task.

As mentioned before, the single case in which the airplane was not able to successfully negotiate the obstacle course occurred on the environment shown at the bottom of Figure 15. This failure can be attributed to the fact that the planner chose to execute one of a small handful of maneuvers that are more aggressive than the funnel we validated in Section 7.2.4. The controller saturates the control inputs significantly on this maneuver and hence violates our assumption about input limits not being reached. Hence this funnel is not entirely valid on the hardware, thus motivating the need to take into account input saturations in a more thorough treatment of the system.

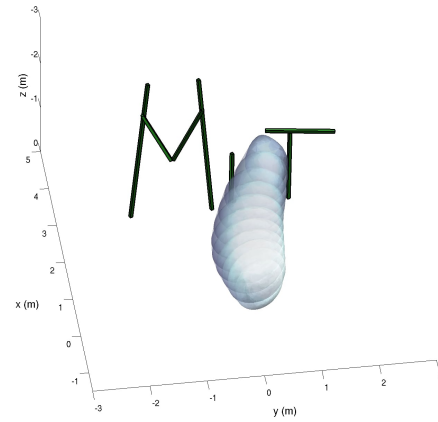
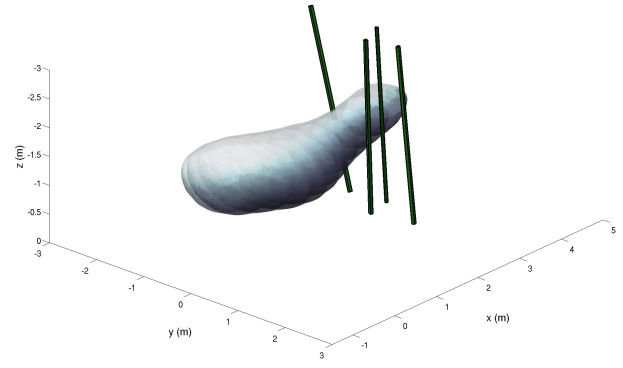
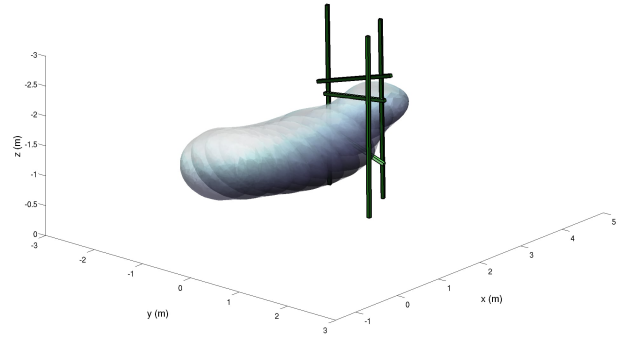
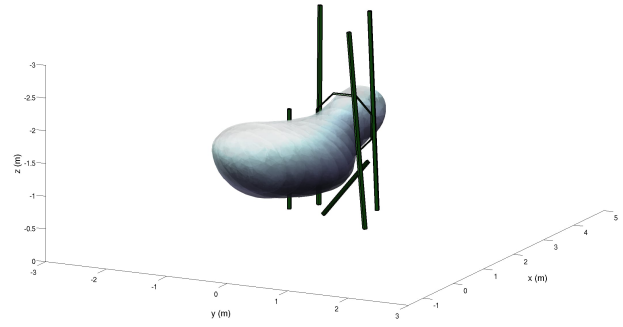
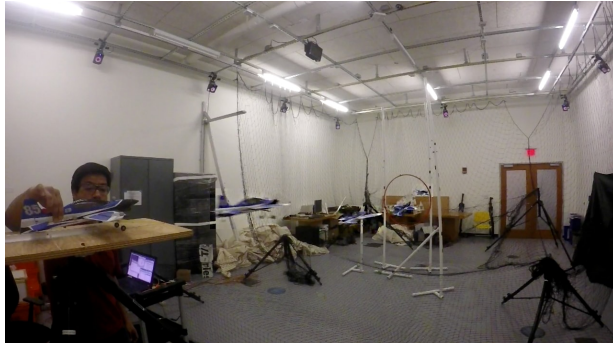


Figure 17: This figure depicts the planned funnel along with the polygonal obstacle representations for four of our fifteen test environments. Note that the funnels have been inflated to take into account the collision geometry of the airplane (modeled as a sphere of diameter equal to the wingspan).



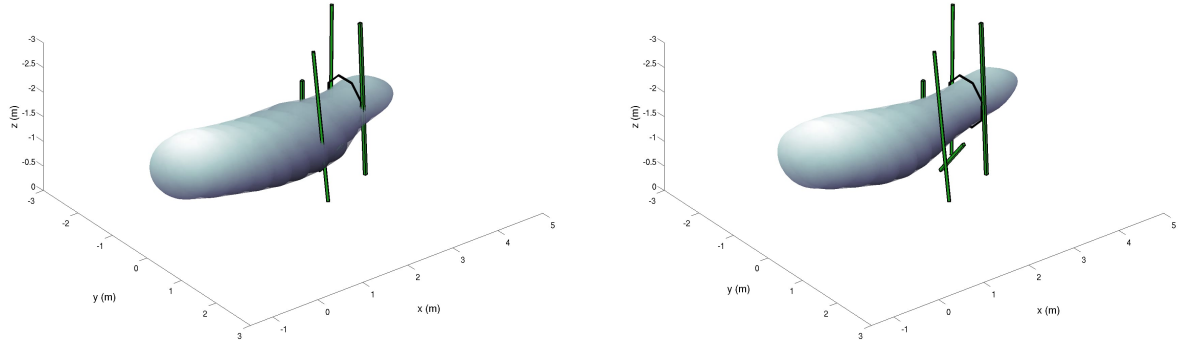


Figure 18: The QCQP-based algorithm for shifting funnels (Section 6.1) plays a crucial role in the planner’s ability to find collision free funnels. Here we compare the output of the planner with and without applying the QCQP-based algorithm for shifting funnels. The best funnel found in the former case is well in collision with the obstacles while in the latter case the planner is able to find a collision free funnel. Note that the funnels chosen in the different cases correspond to different maneuvers.

Finally, we note that on a small number of occasions during our experiments we observed the “failsafe” option being employed by the planner (i.e., switching off the throttle and gliding to a halt). This was typically caused by failures in the launching mechanism such as the airplane making contact with the operator’s hand on its way out of the launcher. Due to the altered initial conditions in these cases the airplane is not in the inlet of most or all of the funnels and thus has to resort to the failsafe. On these occasions we simply repeated the experiment to obtain a successful flight.

## 7.2.6 Implementation details

We end this section by mentioning a few implementation details that were important in achieving the results presented above. First, while the Vicon motion tracking system provides accurate position and orientation estimates at 120 Hz, a finite difference of these measurements can lead to noisy estimates of the derivative states. For our experiments we filtered the finite differences using a simple Luenberger observer [Luenberger, 1971].

Second, we observed a delay of approximately 55 ms in our closed-loop hardware system. While there are several ways to explicitly take this into account by adding delay states to our airplane model, we accommodate for the delay during execution by simulating our model forwards by 55 ms from the estimated current state and using this simulated future state to compute the current control input. This simple strategy is a common one and has previously been found to be effective in a wide range of applications [Horiuchi et al., 1999, Moore et al., 2014, Sipahi et al., 2012].

## 8 Conclusion

In this paper we have presented an approach for real-time motion planning in a priori unknown environments with dynamic uncertainty in the form of bounded parametric model uncertainty and external disturbances. The method augments the traditional trajectory library approach by constructing stabilizing controllers around the nominal trajectories in a library and computing outer approximations of reachable sets (funnels) for the resulting closed-loop controllers via sums-of-squares

(SOS) programming. The pre-computed funnel library is then used to plan online by sequentially composing them together in a manner that ensures obstacles are avoided. We have demonstrated our approach using extensive simulation experiments on a ground vehicle model. These experiments demonstrate that our approach can afford significant advantages over a trajectory-based approach. We have also validated our approach using thorough hardware experiments on a small fixed-wing airplane flying through previously unseen cluttered environments at high speeds.

## Acknowledgements

This work was supported by ONR MURI grant N00014-09-1-1051. The authors would like to thank Michael Posa for help formulating the QCQP presented in Section 6.1, Adam Bry and Charlie Richter for help setting up the USB RC transmitter used in the experiments described in Section 7.2, and the members of the Robot Locomotion Group for many helpful discussions.

## References

- [Ben-Tal and Nemirovski, 2001] Ben-Tal, A. and Nemirovski, A. (2001). *Lectures on modern convex optimization: analysis, algorithms, and engineering applications*, volume 2. SIAM.
- [Berenson et al., 2007] Berenson, D., Diankov, R., Nishiwaki, K., Kagami, S., and Kuffner, J. (2007). Grasp planning in complex scenes. In *International Conference on Humanoid Robots*, pages 42–48. IEEE.
- [Betts, 2001] Betts, J. T. (2001). *Practical Methods for Optimal Control Using Nonlinear Programming*. SIAM Advances in Design and Control. Society for Industrial and Applied Mathematics.
- [Blekherman et al., 2013] Blekherman, G., Parrilo, P. A., and Thomas, R. R. (2013). *Semidefinite optimization and convex algebraic geometry*, volume 13. SIAM.
- [Boyd and Vandenberghe, 2004] Boyd, S. and Vandenberghe, L. (2004). *Convex Optimization*. Cambridge University Press.
- [Brown, 2003] Brown, C. W. (2003). QEPCAD B: A program for computing with semi-algebraic sets using CADs. *ACM SIGSAM Bulletin*, 37(4):97–108.
- [Bry and Roy, 2011] Bry, A. and Roy, N. (2011). Rapidly-exploring random belief trees for motion planning under uncertainty. In *Proceedings of the IEEE International Conference on Robotics and Automation*, Shanghai, China.
- [Burridge et al., 1999] Burridge, R. R., Rizzi, A. A., and Koditschek, D. E. (1999). Sequential composition of dynamically dexterous robot behaviors. *International Journal of Robotics Research*, 18(6):534–555.
- [Collins and Hong, 1998] Collins, G. E. and Hong, H. (1998). *Partial cylindrical algebraic decomposition for quantifier elimination*. Springer.
- [Coumans et al., 2014] Coumans, E. et al. (2014). Bullet physics library. *bulletphysics.org*, 4(6).

- [Dey et al., 2011] Dey, D., Liu, T., Sofman, B., and Bagnell, D. (2011). Efficient optimization of control libraries. Technical report, Technical Report (CMU-RI-TR-11-20).
- [Domahidi and Jerez, 2014] Domahidi, A. and Jerez, J. (2014). FORCES Professional. Embotech GmbH (<http://embotech.com/FORCES-Pro>).
- [Dubins, 1957] Dubins, L. (1957). On curves of minimal length with a constraint on average curvature, and with prescribed initial and terminal positions and tangents. *American Journal of Mathematics*, 79(3):497–516.
- [Frazzoli et al., 2005] Frazzoli, E., Dahleh, M., and Feron, E. (2005). Maneuver-based motion planning for nonlinear systems with symmetries. *IEEE Transactions on Robotics*, 21(6):1077–1091.
- [Frazzoli et al., 2002] Frazzoli, E., Dahleh, M. A., and Feron, E. (2002). Real-Time Motion Planning for Agile Autonomous Vehicles. *Journal of Guidance, Control, and Dynamics*, 25(1):116–129.
- [Gao et al., 2013] Gao, S., Kong, S., and Clarke, E. M. (2013). dReal: An SMT solver for nonlinear theories over the reals. In *Automated Deduction—CADE-24*, pages 208–214. Springer.
- [Gillula et al., 2010] Gillula, J., Huang, H., Vitus, M., and Tomlin, C. (2010). Design of guaranteed safe maneuvers using reachable sets: Autonomous quadrotor aerobatics in theory and practice. In *IEEE International Conference on Robotics and Automation (ICRA)*, pages 1649–1654. IEEE.
- [Green and Kelly, 2007] Green, C. and Kelly, A. (2007). Toward optimal sampling in the space of paths. In *13th International Symposium of Robotics Research*.
- [Horiuchi et al., 1999] Horiuchi, T., Inoue, M., Konno, T., and Namita, Y. (1999). Real-time hybrid experimental system with actuator delay compensation and its application to a piping system with energy absorber. *Earthquake Engineering & Structural Dynamics*, 28(10):1121–1141.
- [Jacobs and Canny, 1990] Jacobs, P. and Canny, J. (1990). Robust motion planning for mobile robots. In *Robotics and Automation, 1990. Proceedings., 1990 IEEE International Conference on*, pages 2–7. IEEE.
- [Karaman and Frazzoli, 2011] Karaman, S. and Frazzoli, E. (2011). Sampling-based algorithms for optimal motion planning. *Int. Journal of Robotics Research*, 30:846–894.
- [Kuffner and Lavalley, 2000] Kuffner, J. and Lavalley, S. (2000). RRT-connect: An efficient approach to single-query path planning. In *Proceedings of the IEEE International Conference on Robotics and Automation (ICRA)*, pages 995–1001.
- [Liu and Atkeson, 2009] Liu, C. and Atkeson, C. (2009). Standing balance control using a trajectory library. In *Intelligent Robots and Systems, 2009. IROS 2009. IEEE/RSJ International Conference on*, pages 3031–3036. IEEE.
- [Ljung, 2007] Ljung, L. (2007). System identification toolbox for use with matlab.
- [Luenberger, 1971] Luenberger, D. (1971). An introduction to observers. *Automatic Control, IEEE Transactions on*, 16(6):596–602.

- [Majumdar et al., 2013] Majumdar, A., Ahmadi, A. A., and Tedrake, R. (2013). Control design along trajectories with sums of squares programming. In *Proceedings of the 2013 IEEE International Conference on Robotics and Automation (ICRA)*, pages 4054–4061.
- [Majumdar and Tedrake, 2012] Majumdar, A. and Tedrake, R. (2012). Robust online motion planning with regions of finite time invariance. In *Proceedings of the Workshop on the Algorithmic Foundations of Robotics*, page 16, Cambridge, MA.
- [Mayne et al., 2005] Mayne, D., Seron, M., and Rakovic, S. (2005). Robust model predictive control of constrained linear systems with bounded disturbances. *Automatica*, 41(2):219–224.
- [Mitchell et al., 2005] Mitchell, I., Bayen, A., and Tomlin, C. (2005). A time-dependent hamilton-jacobi formulation of reachable sets for continuous dynamic games. *IEEE Transactions on Automatic Control*, 50(7):947–957.
- [Moore, 2014] Moore, J. (2014). *Robust Post-Stall Perching with a Fixed-Wing UAV*. PhD thesis, Massachusetts Institute of Technology.
- [Moore et al., 2014] Moore, J., Cory, R., and Tedrake, R. (2014). Robust post-stall perching with a simple fixed-wing glider using lqr-trees. *Bioinspiration and Biomimetics*, 9(2):15.
- [Ny and Pappas, 2012] Ny, J. L. and Pappas, G. (2012). Sequential composition of robust controller specifications. In *International Conference on Robotics and Automation (ICRA)*. IEEE.
- [Parrilo, 2000] Parrilo, P. A. (2000). *Structured Semidefinite Programs and Semialgebraic Geometry Methods in Robustness and Optimization*. PhD thesis, California Institute of Technology.
- [Platt et al., 2012] Platt, R., Kaelbling, L., Lozano-Perez, T., and Tedrake, R. (2012). Non-gaussian belief space planning: Correctness and complexity. In *Proceedings of the 2012 IEEE International Conference on Robotics and Automation (ICRA)*.
- [Platt et al., 2010] Platt, R., Tedrake, R., Kaelbling, L., and Lozano-Perez, T. (2010). Belief space planning assuming maximum likelihood observations. In *Proceedings of Robotics: Science and Systems*.
- [Schouwenaars et al., 2003] Schouwenaars, T., Mettler, B., Feron, E., and How, J. (2003). Robust motion planning using a maneuver automation with built-in uncertainties. In *American Control Conference, 2003. Proceedings of the 2003*, volume 3, pages 2211–2216. IEEE.
- [Sermanet et al., 2008] Sermanet, P., Scoffier, M., Crudele, C., Muller, U., and LeCun, Y. (2008). Learning maneuver dictionaries for ground robot planning. In *Proc. 39th International Symposium on Robotics (ISR08)*.
- [Shkolnik, 2010] Shkolnik, A. (2010). *Sample-Based Motion Planning in High-Dimensional and Differentially-Constrained Systems*. PhD thesis, MIT.
- [Sipahi et al., 2012] Sipahi, R., Vyhlídal, T., Niculescu, S.-I., and Pepe, P. (2012). *Time Delay Systems: Methods, Applications and New Trends*, volume 423. Springer.



- [Sobolic, 2009] Sobolic, F. M. (2009). Agile flight control techniques for a fixed-wing aircraft. Master’s thesis, Massachusetts Institute of Technology, Department of Aeronautics and Astronautics, Cambridge MA.
- [Stevens and Lewis, 1992] Stevens, B. and Lewis, F. (1992). *Aircraft Control and Simulation*. John Wiley & Sons, Inc.
- [Stolle and Atkeson, 2006] Stolle, M. and Atkeson, C. (2006). Policies based on trajectory libraries. In *Proceedings of the International Conference on Robotics and Automation (ICRA)*. IEEE.
- [Tedrake et al., 2010] Tedrake, R., Manchester, I. R., Tobenkin, M. M., and Roberts, J. W. (2010). LQR-Trees: Feedback motion planning via sums of squares verification. *International Journal of Robotics Research*, 29:1038–1052.
- [Tobenkin et al., 2011] Tobenkin, M. M., Manchester, I. R., and Tedrake, R. (2011). Invariant funnels around trajectories using sum-of-squares programming. *Proceedings of the 18th IFAC World Congress, extended version available online: arXiv:1010.3013 [math.DS]*.
- [Vandenberghe and Boyd, 1996] Vandenberghe, L. and Boyd, S. (1996). Semidefinite programming. *SIAM Review*, 38(1):49–95.